

Article

Research on Mooring System Design for Kulluk Platform in Arctic Region

Aobo Zhang, Zhenju Chuang *, Shewen Liu, Xin Chang, Lixun Hou, Zhen He and Shiqi Liu

School of Naval Architecture and Ocean Engineering, Dalian Maritime University, Dalian 116026, China; zhangao@dlmu.edu.cn (A.Z.); liushewen@dlmu.edu.cn (S.L.); xin.chang@dlmu.edu.cn (X.C.); houlixun@dlmu.edu.cn (L.H.); xiaohao@dlmu.edu.cn (Z.H.); liushiqi456@dlmu.edu.cn (S.L.)

* Correspondence: zhenjuchuang@dlmu.edu.cn

Abstract: Mooring system design of a floating offshore structure in the arctic region is considered to be extremely important. This paper aims at investigating an optimal mooring system for the Kulluk platform operating in the Beaufort Sea, which has ice-free and ice-covered conditions during the whole year time. In order to complete the layout design of the mooring system to satisfy the year-round operation, both the effect of wave loads and ice loads should be considered. The research establishes a coupled numerical production system composed of the Kulluk platform and mooring system. Wave load is solved by potential flow theory. The slender finite element method is used to compute the tension of the mooring system. The nonlinear finite element method, discrete element method, and empirical formula are compared to analyze ice load. Finally, the discrete element method is selected for the analysis of the Kulluk, and the simulated results are compared reasonably with the field data. When studying the mooring line configurations, quantitative time-domain analysis is carried out, including tension of mooring lines and the motions of the platform under different working conditions. The research work in this paper will provide a reference for the optimal design of the mooring system of the platform operating in the Arctic Sea.

Keywords: arctic oil and gas resources; Kulluk platform; mooring system; ice load; ice-structure interaction



Citation: Zhang, A.; Chuang, Z.; Liu, S.; Chang, X.; Hou, L.; He, Z.; Liu, S. Research on Mooring System Design for Kulluk Platform in Arctic Region. *Water* **2022**, *14*, 1762. <https://doi.org/10.3390/w14111762>

Academic Editors: Zhijun Li, Tomasz Kolerski, Xiaohong Shi, Zhengyong Zhang and Li Zhou

Received: 30 April 2022

Accepted: 28 May 2022

Published: 30 May 2022

Publisher's Note: MDPI stays neutral with regard to jurisdictional claims in published maps and institutional affiliations.



Copyright: © 2022 by the authors. Licensee MDPI, Basel, Switzerland. This article is an open access article distributed under the terms and conditions of the Creative Commons Attribution (CC BY) license (<https://creativecommons.org/licenses/by/4.0/>).

1. Introduction

At present, the resources on land are becoming fewer and fewer, and the sea contains a large number of available resources. Exploring and exploiting offshore oil and gas resources has excellent development potential, especially in the Arctic region. The cover and thickness of sea ice in the Arctic region have decreased significantly due to global warming, which is conducive to the exploitation of oil and gas resources in the Arctic region. However, petroleum exploration in the Arctic region is extremely challenging. The difficulty is that a large amount of undiscovered oil is stored in water depths greater than 100 m [1] and less than 500 m [2]. Coupled with the impact of sea ice on structures, exploration of oil and gas resources in the polar regions has not become a normal state.

Kulluk platform operated as a drilling system in the Beaufort Sea from 1983 to 1993. A large number of platform-related data were monitored in real-time. Kulluk's hull has good ice resistance, and its motion response and the tension of the mooring lines is less than other structures. Kulluk's experience provides a data source for analyzing moored structures under different sea ice conditions [3]. Zhou et al. [4] verified the effectiveness of the numerical model by comparing the simulation results of the two-dimensional numerical model with the field data of the Kulluk platform. For moored structures, ice thickness, ice drift speed, and global mooring stiffness affect the platform's motion and the tension of mooring lines. Sayed and Barker [5] described a numerical model based on mass and momentum conservation equations, sea ice constitutive equation, and moored structure motion equation. This model simulated the interaction between the broken ice floe and the

Kulluk platform and studied the influence of mooring stiffness. Fluid–structure interaction (FSI) can be used to analyze moored structures under broken ice floes [6]. This study simulated platform motion at different ice concentrations (low, medium, and high) and compared it with full-scale field data.

A mooring system can improve the stability of floating structures, so it becomes a critical component in the design. The positioning modes of floating structures mainly include a mooring system and a dynamic positioning system. The mooring system is the most common positioning method, and the thruster-assisted mooring system has become the research hotspot. Floating structures and their mooring systems are exposed to the ocean environment throughout their service lives. When the horizontal displacement of the connected floating frame exceeds the limited value, the entire mooring system will experience functional failure [7]. Garrett [8] presented a fully coupled global analysis of floating production systems, including structures, mooring systems, and riser systems. This study provided accuracy and efficiency for a fully coupled analysis of floating production system design from concept selection to final design, installation, and operation. O.A. Montasir [9] studied the difference between symmetric and asymmetric multi-point mooring configurations on structural motion and evaluated the mooring recovery force-displacement relationship of truss SPAR platform with a quasi-static method. Finally, the linear airy wave theory and Morrison equation were used to calculate the platform motion under waves. The influence of mooring line configurations on platform motion response was analyzed. Mohapatra and Guedes Soares [10] studied the hydroelastic response of the moored floating flexible plate by analyzing the effects of the mooring stiffness, incidence angle, and flexural rigidity on the deflection amplitude, plate deformations, reflection, and transmission coefficients.

With the increasing importance of oil and gas resources in the Arctic region, eliminating ice load damage to offshore platform structures has become a research focus. More and more scholars have carried out an in-depth analysis of the interaction between sea ice and the platform. Horrigmoe et al. [11] used the nonlinear finite element method to numerically calculate the ice loads based on the viscoplastic constitutive model for ice. Considering the elastic, creep, and plastic components of the strain of ice, the strain rate in a wide range can be predicted to calculate the force of ice on structures. A simple ice indentation test verified the numerical model under plane stress conditions. Hansen and Loset [12] used a two-dimensional disk element to simulate a broken ice floe, analyzed the moored structure's motion response under ice floes, and compared it with the ice pool test. This numerical simulation introduced the friction coefficient to consider friction action. Liu et al. [13] proposed an ideal elastic-plastic ice model to simulate an actual ship-iceberg collision and compared the simulated contact pressure-contact area curve with the design specification to verify the feasibility of the model. Liu and Ji [14] used the dilated polyhedral elements based on the Minkowski sum theory to describe the geometry of irregular particle elements and adopted the 2D-Voronoi tessellation algorithm to obtain the initial random distribution state of ice floes. The ice load of the Kulluk platform was analyzed by the discrete element method.

This study compares the numerical data with the field data to obtain more accurate ice load simulation results. The motion response of the Kulluk platform coupled with the mooring system is computed under wave load and ice load, respectively. The influence of wave, level ice, and ice floes on platform motion and mooring line tension is considered comprehensively. In this research, the three methods of nonlinear finite element, discrete element, and empirical formula are compared to compute ice loads. This paper uses the potential flow theory to calculate wave loads. The slender finite element method is used to analyze the mooring system. The basic principles of static catenary analysis are discussed in catenary element equilibrium equations [15] and catenary equilibrium of multi-segment single lines [16]. The calculation results in the time domain are compared from the load direction, the number of mooring lines, the number of connecting points, and the angle between mooring lines to optimize the mooring system layout design.

2. Theoretical Background

2.1. Calculation Method of Wave Loads

Kulluk platform is a large-scale structure. Considering wave diffraction and radiation effects, potential flow theory [17] is used to analyze the wave loads. SESAM software performs the platform’s hydrodynamic characteristics and the structural motion response [18]. The WADAM module [19] can analyze the response in the frequency domain under wave loads. The transfer function RAO, first-order wave force, and second-order mean drift force can be obtained through computation. The SIMA module [20] can be used to analyze the time-domain response of the Kulluk coupled with the mooring system. In the study of the Kulluk platform, its flexible deformation is ignored, and it is regarded as a rigid body when solving its six6 DOF motions. The OXY plane coincides with the stationary water surface, and the OZ axis is perpendicular to the water surface and points upwards [21].

According to potential flow theory [17], the first-order motion equation of the Kulluk platform in the frequency domain can be formulated:

$$(M_{ij} + \mu_{ij})\ddot{X}_j + \lambda_{ij}\dot{X}_j + C_{ij}X_j = F_i \quad (i = 1, 2, \dots, 6; j = 1, 2, \dots, 6) \tag{1}$$

where, M_{ij} is the mass matrix; μ_{ij} is the additional mass matrix; X_j is the platform’s motion; λ_{ij} is the damping coefficient matrix; C_{ij} is the restoring force coefficient matrix; F_i is the first-order wave force applied to the platform.

2.2. Analysis Method of Ice Loads

The empirical formula, finite element method, and discrete element method are applied to analyze ice loads. This paper studies a cylinder structure and a cone structure under level ice as examples to compare these three research methods. Crushing failure occurs between ice and the vertical structures. Flexure failure usually dominates ice acting on cone structures.

2.2.1. The Empirical Formula of ISO (The International Organization for Standardization)

The ISO-19906(2019) [22] standard is the reference for designing and manufacturing offshore structures in the oil and gas industry.

1. Crushing failure of ice

The calculation formula is:

$$F_G = p_G \cdot h \cdot w \tag{2}$$

$$p_G = C_R \left[\left(\frac{h}{h_1} \right)^n \left(\frac{w}{h} \right)^m + f_{AR} \right] \tag{3}$$

$$f_{AR} = e^{-\frac{w}{3h}} \sqrt{1 + 5 \frac{h}{w}} \tag{4}$$

where p_G is the global average ice pressure; w is the projected width of the structure; h is the thickness of the level ice; h_1 is a reference thickness of 1 m; m is an empirical coefficient equal to -0.16 ; n is an empirical coefficient equal to $-0.5 + h/5$ for $h < 1.0$ m and to -0.3 for $h \geq 1.0$ m; C_R is the ice strength coefficient equal to 2.8 Mpa in the Beaufort Sea.

2. Flexure failure of ice

The ice loads acting on the cone structure include actions due to the flexure failure of the level ice and the ride-up actions due to ice pieces. The horizontal breaking action H_B and the vertical breaking action V_B are given by:

$$H_B = \frac{\sigma_f h^2 \tan \alpha}{3} \frac{1 - \mu g_r}{1 - \mu g_r} \left[\frac{1 + Yx \ln x}{x - 1} + G(x - 1)(x + 2) \right] \tag{5}$$

$$V_B = H_B \cdot h_v \tag{6}$$

where Y is equal to 2.711 for Tresca yielding; $G = \frac{\rho_{ice} g D^2}{4\sigma_f \cdot h}$, $x = 1 + \left(3G + \frac{Y}{2}\right)^{-\frac{1}{2}}$,
 $g_r = \frac{\sin \alpha + \frac{\alpha}{\cos \alpha}}{\frac{\pi}{2} \sin^2 \alpha + 2\mu \alpha \cos \alpha}$.

The horizontal ride-up action H_R and the vertical ride-up action V_R are defined as given by:

$$H_R = W \frac{\tan \alpha + \mu E_2 - \mu f g_r \cos \alpha}{1 - \mu g_r} \quad (7)$$

$$V_R = W \cos \alpha \left(\frac{\pi}{2} \cos \alpha - \mu \alpha - f h_V \right) + H_R h_V \quad (8)$$

$$W = \rho_i g h_r \frac{w^2 - w_T^2}{4 \cos \alpha} \quad (9)$$

$$f = \sin \alpha + \mu E_1 \cos \alpha \quad (10)$$

$$h_V = \frac{f \cos \alpha - \mu E_2}{\frac{\pi}{4} \sin^2 \alpha + \mu \alpha \cos \alpha} \quad (11)$$

$$E_1 = \int_0^{\frac{\pi}{2}} \left(1 - \sin^2 \alpha \sin^2 \eta \right)^{-\frac{1}{2}} d\eta \quad (12)$$

$$E_2 = \int_0^{\frac{\pi}{2}} \left(1 - \sin^2 \alpha \sin^2 \eta \right)^{\frac{1}{2}} d\eta \quad (13)$$

where α is the slope of the structure measured from the horizontal; w_T is the top diameter of the cone; h_r is the ice ride-up thickness ($h_r \geq h$).

The total action components in horizontal and vertical directions are obtained, respectively, by

$$F_H = H_B + H_R \quad (14)$$

$$F_V = V_B + V_R \quad (15)$$

2.2.2. Finite Element Method

The nonlinear explicit dynamics analysis software LS-DYNA [23] has the function of solving fluid–structure interaction. The nonlinear finite element method can divide the research subject into several elements. These elements are connected by nodes that transfer loads between the elements.

1. Ice-structure contact algorithm

Three methods for LS-DYNA are applied to deal with contact collision, including the node constraint method, allocation parameter method, and penalty function method. This paper uses the penalty function method for analysis [24].

The contact force of the penalty function method is: $F = K\delta$,

where K is the contact surface stiffness (determined by element size and material properties); δ is the amount of penetration.

2. Fluid-structure interaction algorithm

LS-DYNA has the Lagrange, Euler, and ALE algorithms according to the various coordinate types. ALE algorithm can perform better dynamic analysis of fluid–structure interaction and combine the Lagrange algorithm and Euler algorithm characteristics. It can track the motion of the structure similarly to the Lagrange algorithm. It can also adjust the position of the mesh according to the demands of the solution to avoid severe deformation of the mesh [25].

LS-DYNA uses penalty function method for fluid dynamics calculation, viscosity coefficient and equation of state (EOS), and null-material model for fluid modeling and

adopts the keyword “CONSTRAINED_LAGRANGE_IN_SOLID” to directly couple solid and fluid elements.

The null material model (*MAT_NULL) is used to simulate the water in conjunction with the equation of state, and viscosity is also defined. Null material models can effectively simulate fluid and hydrodynamic properties. The deviational shear stress of the fluid element σ_d is proportional to the shear strain ϵ' :

$$\sigma_d = 2\mu\epsilon' \tag{16}$$

where μ represents the viscosity of the fluid in Pa·s.

Fluid can be described by the following two equations of state: Gruneisen equation of state and linear polynomial equation of state.

The equation of state of water is described by Gruneisen equation of state. Water is defined as the pressure of the compressed material:

$$p = \frac{\rho_0 C^2 \mu [1 + (1 - \frac{\gamma_0}{2})\mu - \frac{a}{2}\mu^2]}{[1 - (S_1 - 1)\mu - S_2 \frac{\mu^2}{\mu+1} - S_3 \frac{\mu^3}{(\mu+1)^2}]} + (\gamma_0 + \alpha\mu)E \tag{17}$$

where P is pressure; C is the intercept of impact velocity V_x - particle velocity V_p curve; S_1 , S_2 and S_3 are the coefficients of slope of V_x - V_p curve; γ_0 is the Gruneisen constant; α is the first-order volume correction of γ_0 .

The equation of state of air is described by the linear polynomial equation of state. The linear polynomial equation of state represents the linear relationship of internal energy per unit initial volume. The pressure value is given by the following equation:

$$p = C_0 + C_1\mu + C_2\mu^2 + C_3\mu^3 + (C_4 + C_5\mu + C_6\mu^2)E \tag{18}$$

where $C_0, C_1, C_2, C_3, C_4, C_5$, and C_6 are constants; if $\mu < 0$, then $C_2\mu^2$ and $C_6\mu^2$ are set to 0, where:

$$\mu = \frac{1}{V} - 1 \tag{19}$$

where V represents the relative volume.

The specific calculation parameters are shown in Tables 1–3.

Table 1. Main parameters of the structure in finite element calculation.

Mass Density	Young’s Modulus	Poisson’s Ratio
7850 kg/m ³	206 Gpa	0.3

Table 2. Main parameters of level ice in finite element calculation.

Mass Density	Shear Modulus	Yield Stress	Plastic Hardening Modulus	Bulk Modulus	Failure Pressure	Plastic Failure Strain
900 kg/m ³	2.2 Gpa	2.12 Mpa	4.26 Gpa	5.26 Gpa	−4 Mpa	0.35

Table 3. Main parameters of water and air in finite element calculation.

	State Equation	Density	Viscosity Coefficient	Failure Pressure
Air	*EOS_LINEAR_POLYNOMIAL	1.25 kg/m ³	1.74 × 10 ^{−5}	−10 Mpa
Water	*EOS_GRUNEISEN	1000 kg/m ³	0.9 × 10 ^{−3}	−10 Mpa

2.2.3. Discrete Element Method

The discrete element method [26] uses a parallel bond model to simulate level ice composed of spherical particles. An elastic bonding disk is between the two bonding particles, namely transforming forces and moments [27]. The parallel bond model is shown in Figure 1:

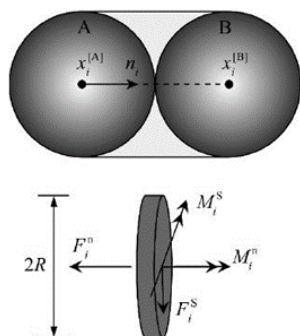


Figure 1. Parallel bonding model for spherical elements.

In the parallel bonding model, \vec{F}_i^n and \vec{F}_i^s are, respectively, the normal force and tangential force between particles; M_i^n and M_i^s are, respectively, the normal moment and tangential moment between particles. The maximum normal stress and maximum shear stress acting on the bonding disk can be expressed as [28]:

$$\sigma_{\max} = \frac{\vec{F}_i^n}{A} + \frac{\left| \vec{M}_i^s \right|}{I} R \tag{20}$$

$$\tau_{\max} = \frac{\vec{F}_i^s}{A} + \frac{\left| \vec{M}_i^n \right|}{J} R \tag{21}$$

where R is the radius of the bonding disk, A is the cross-sectional area of the bonding disk, and I and J are the moment of inertia and polar moment of inertia of the bonding disk, respectively. The specific formula can be expressed as: $A = \pi R^2, J = \frac{1}{2} \pi R^4, I = \frac{1}{4} \pi R^4$.

The bonding failure model of particles is divided into tensile failure and shear failure [28], as demonstrated in Figure 2. When the fracture of ice is simulated, and the maximum stress on the bonding disk exceeds the strength of bonding failure, the fracture criterion appears, as described in Figure 3.

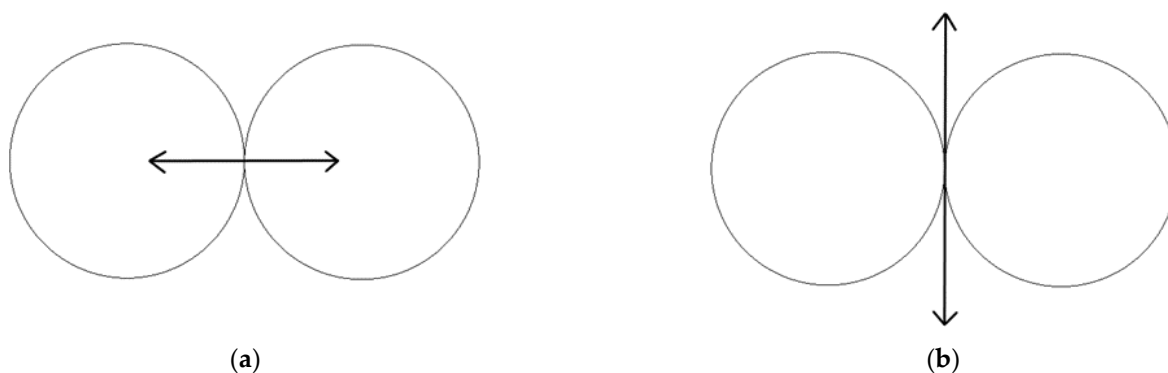


Figure 2. Bonding failure model of particle element. (a) Tensile failure; (b) shear failure.

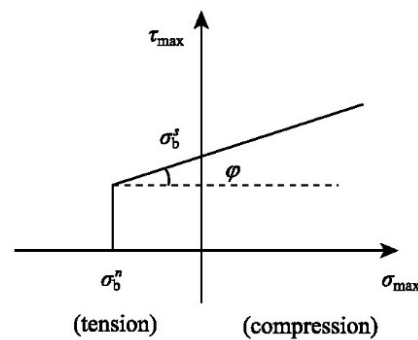


Figure 3. Fracture criterion with tensile and shear failure.

The tensile failure strength σ^t and shear failure strength τ^s of the bonding elements can be expressed as [29]:

$$\sigma^t = \sigma_b^n \tag{22}$$

$$\tau^s = \sigma_b^s + \mu_b \sigma_{\max} \tag{23}$$

where σ_b^n and σ_b^s denote the normal bonding strength and tangential bonding strength, respectively. In this paper, $\sigma_b^n = \sigma_b^s$. μ_b is the internal friction coefficient; $\mu_b = \tan \varphi$. φ is the internal friction angle.

This paper uses the discrete element method to analyze the broken ice floes condition. A two-dimensional Voronoi tessellation algorithm [30] constructs the ice fragmentation regions with different ice thickness, ice concentration, and average ice area. A Voronoi diagram, also known as a Dirichlet diagram or Tyson polygon, is a set of continuous polygons consisting of vertical bisects connected by two adjacent points. The algorithms of constructing Voronoi graph generally include divide and conquer method, plane scanning method, and definition method based on Delaunay triangulation. The two-dimensional Delaunay triangulation method divides a two-dimensional plane into random polygons [15]. The area of broken ice floes is depicted in Figure 4. The calculation parameters are shown in Table 4.

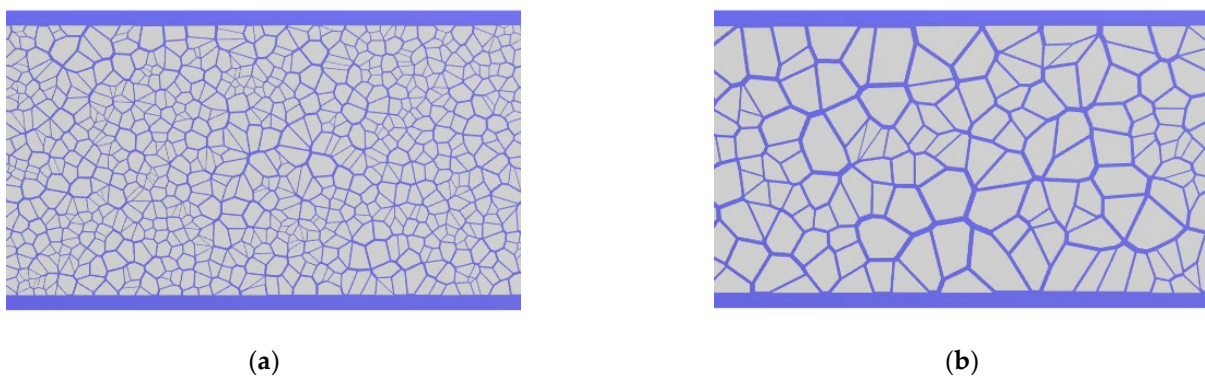


Figure 4. Schematic diagram of broken ice floes area under different conditions: (a) 80% ice concentration, the average area of 20 m² of ice floes condition; (b) 80% ice concentration, the average area of 100 m² of ice floes condition.

Table 4. Main parameters of sea ice discrete element calculation.

Parameter	Symbol	Value	Unit
Elastic modulus	E	1.0	GPa
The density of water	ρ_w	1035.0	kg/m ³
The density of ice	ρ_i	920.0	kg/m ³

Table 4. Cont.

Parameter	Symbol	Value	Unit
The friction coefficient of particle element	μ_b	0.25	—
The friction coefficient between sea ice and structure	μ_s	0.25	—
Particle normal bond strength	σ_b^n	1.57	—
Particle tangential bond strength	σ_b^s	1.57	—
Particle compression strength	σ_c	2.53	MPa

3. Comparison of Ice Load Calculation Methods

The failure modes of ice include crushing failure and flexure failure. This paper adopts the nonlinear finite element method (FEM) and discrete element method (DEM) to simulate the crushing failure between ice and cylinder as well as the flexure failure between ice and cone structure, respectively. The simulation process can be observed in Figures 5 and 6. The figures reveal that both methods can reasonably simulate the interaction between ice and structures.

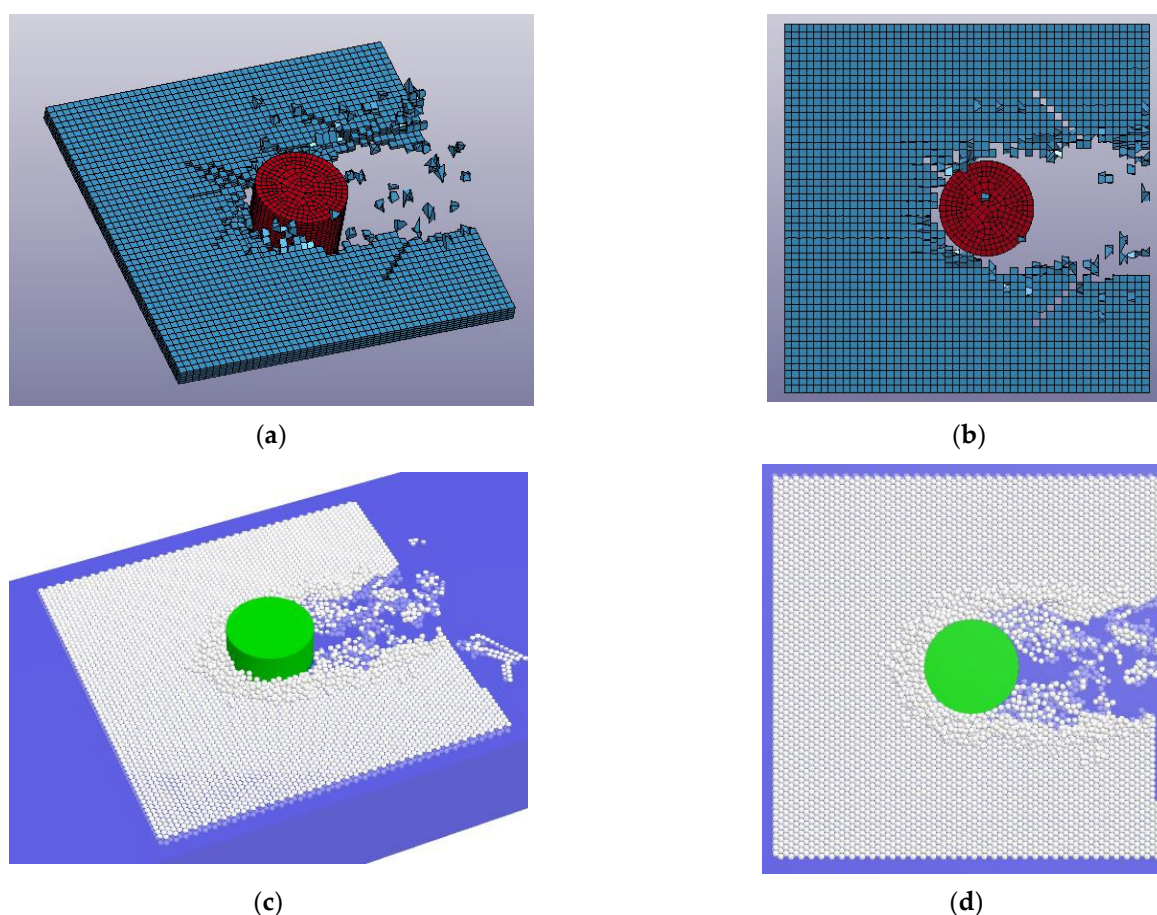


Figure 5. Simulation of interaction between cylinder structure and level ice. (a) Schematic diagram of finite element method calculation; (b) top view of finite element method calculation; (c) schematic diagram of discrete element method calculation; (d) top view of discrete element method calculation.

Figure 7 describes the ice load values under the same ice condition for cylinder and cone structures obtained by different methods. The two simulation methods' time history curves of ice load show irregular trend fluctuation, and the peak value appears almost simultaneously. The difference is that the peak value of the ice loads obtained by the finite element method is more significant than that computed by the discrete element method, especially in crushing failure, and the difference is more than 100%. The fluid does not act

as a buffer in finite element analysis. It will create a more significant force when ice contacts the structure. The setting of erosion contact makes less impact frequency between ice and structures. Therefore, the finite element method results in a more considerable ice-loads fluctuation than the discrete element method.

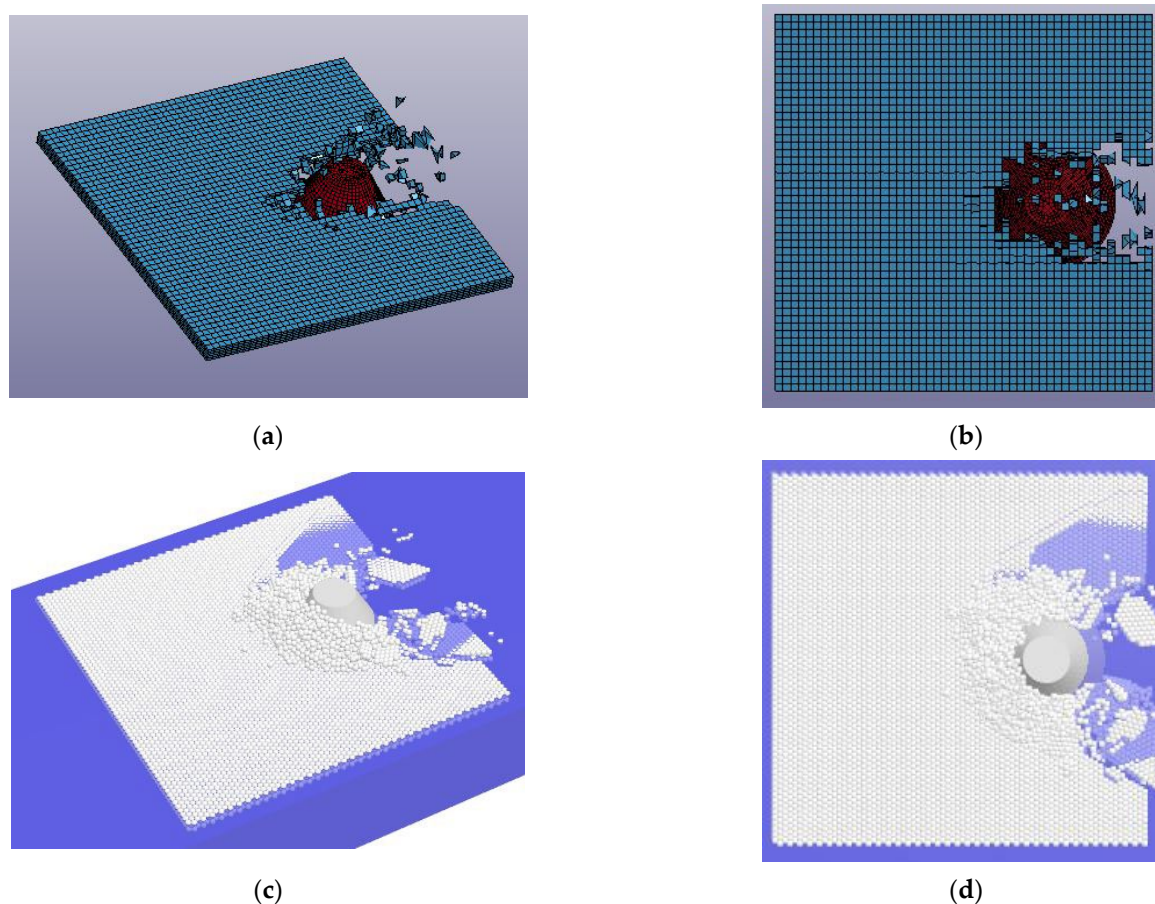


Figure 6. Simulation of interaction between cone structure and level ice. (a) Schematic diagram of finite element method calculation; (b) top view of finite element method calculation; (c) schematic diagram of discrete element method calculation; (d) top view of discrete element method calculation.

The numerical values of the nonlinear finite element method, discrete element method, and empirical formula are compared by statistics. The research object is the average values and standard deviation of ice loads at different ice speeds (0.1–0.5 m/s) at the same ice thickness (2 m). Analyzing the calculation results of single ice speed causes a shortage of statistical samples, which cannot guarantee its reliability. Therefore, several groups of ice speed data are selected for statistical analysis. Table 5 shows the numerical comparison of different ice load analysis methods.

The results of the discrete element method are relatively small for crushing failure, while the results of the finite element method are close to those of the empirical formula. In the analysis of flexure failure, there is little difference between these three methods. The average value of DEM method is closer to the empirical formula, and the standard deviation is smaller. Meanwhile, considering the calculation's accuracy and time, the discrete element is a more suitable method. The Kulluk platform contacts with ice as a cone structure, in which flexure failure happens. In this paper, the discrete element method is applied to analyze the ice loads of the Kulluk under the conditions of level ice and broken ice floes.

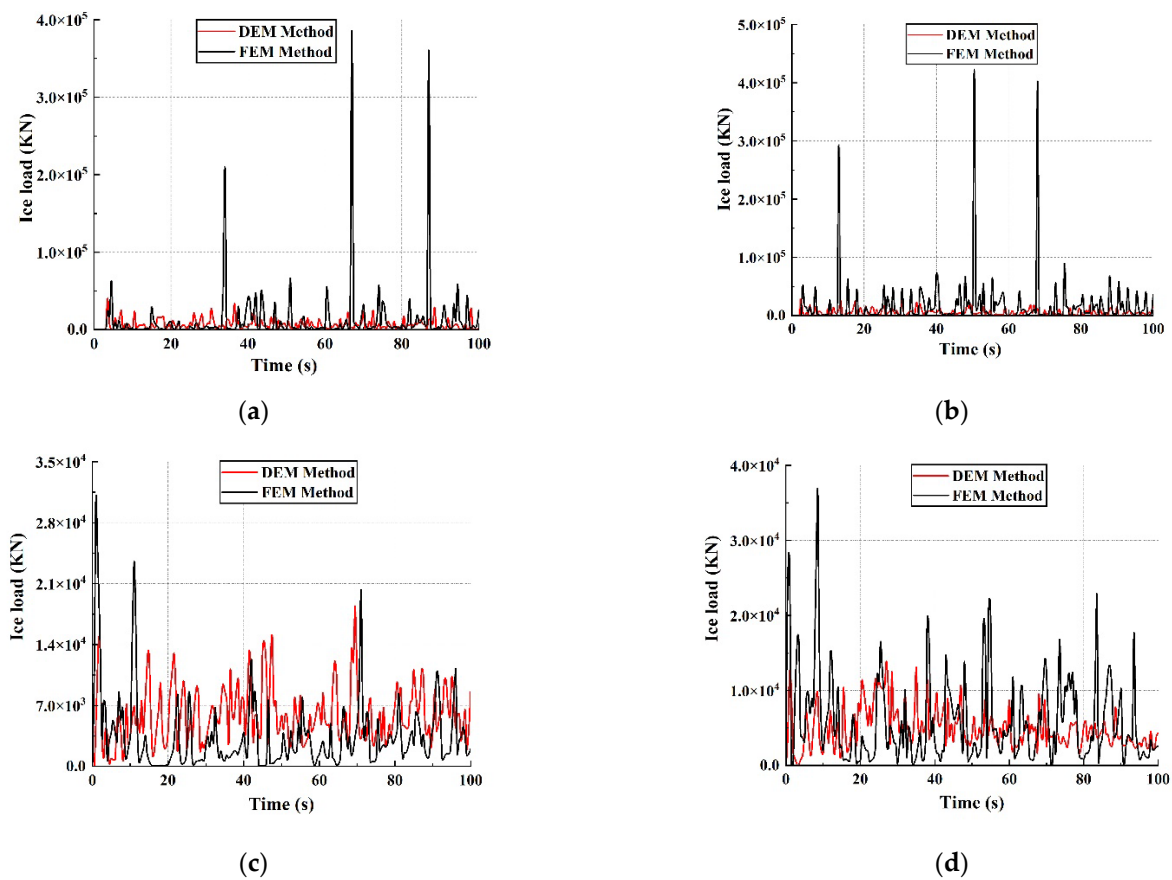


Figure 7. Numerical comparison of ice load between finite element method and discrete element method. (a) Cylinder structure at 0.3 m/s ice speed; (b) cylinder structure at 0.4 m/s ice speed; (c) cone structure at 0.2 m/s ice speed; (d) cone structure at 0.4 m/s ice speed.

Table 5. The numerical comparison of different ice load analysis methods.

	Ice Speed (m/s)					Average Value	Standard Deviation	Empirical Formula
	0.1	0.2	0.3	0.4	0.5			
DEM—cylinder structure	6007.58 kN	6983.78 kN	7717.35 kN	8386.42 kN	9063 kN	7273.78 kN	1124.58	26,343.32 kN
FEM—cylinder structure	9043.24 kN	13,120.88 kN	18,343.52 kN	19,272.79 kN	20,634.68 kN	16,083.02 kN	4343.61	
DEM—cone structure	4959.72 kN	5285.41 kN	5625.54 kN	5981.75 kN	6018.99 kN	5574.28 kN	406.83	6600 kN
FEM—cone structure	2869.34 kN	3451.97 kN	4971.67 kN	5863.48 kN	6226.38 kN	4676.57 kN	1316.32	

4. Numerical Model and Environmental Conditions

This paper selects the full-scale Kulluk platform as the numerical model, as displayed in Figure 8. The Kulluk is a symmetrical structure with a downward sloping circular hull that resists environmental loads in all directions. Table 6 lists the specific design parameters.

The mooring system is the research focus of this paper. In the numerical simulation, fairleads connection and supernodes are defined to establish a fully coupled system between the Kulluk platform and the mooring system. The mooring system is arranged by radial symmetry. Together with the circular structure, it can resist loads in any direction. The Kulluk platform’s mooring lines are located below the waterline to eliminate collisions between ice and mooring lines at the waterline.

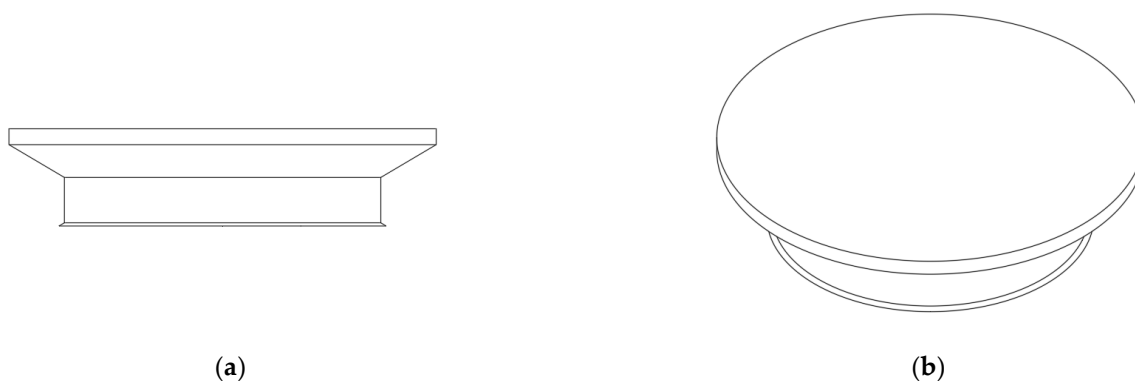


Figure 8. Numerical computation model of Kulluk platform. (a) Front view of the model; (b) stereogram of the model.

Table 6. Basic parameters of the Kulluk platform.

Parameter	Value	Unit
Top diameter	81	m
Diameter at waterline	67.5	m
Bottom diameter	60	m
Depth	18.4	m
Draft	11.5	m
Displacement	28,000	m ³
Cone angle	31.4	°

Figure 9 depicts the specific location of the Beaufort Sea. It is located in latitude 69° N to 75° N and longitude 125° W–152° W. The length of the ice-covered season is early October to late July. The length of the open water season is August to early October. ISO 19906(2019) [22] provides detailed information about the Beaufort Sea environment, including wind, wave, current, and ice data. The research direction of this paper is the arrangement of the mooring system rather than analyzing the influence of environmental factors. Therefore, wave, level ice, and broken ice floes are computed under a single working condition. The operating conditions selected in this paper are as follows: Significant wave height is 3.7 m, and the spectral peak period is 6.7 s. The current velocity is 0.4 m/s. The thickness of level ice is 2 m, and the ice speed is 0.08 m/s. Under the condition of broken ice floes, the thickness of the ice floes is 2 m, the average size of ice floes is 100 m², and the broken ice concentration is 80%.

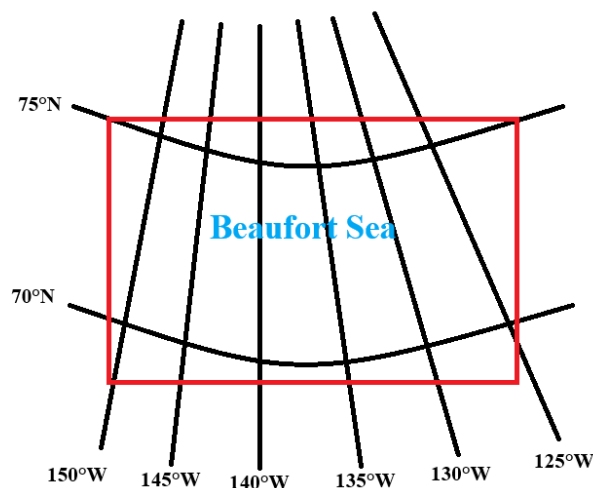


Figure 9. The geographical location of the Beaufort Sea [22].

5. Hydrodynamic Analysis of the Kulluk Platform

The motion transfer function RAO, first-order wave forces, and second-order wave forces of the Kulluk platform should be analyzed. The linear first-order wave force is obtained by factoring the velocity potential into the incident potential, diffraction potential, and radiation potential using Bernoulli's equation. The second-order mean drift force is a nonlinear force that affects the mooring system. There are two methods for computation: the far-field method [31] and the direct pressure integral method [32]. The Kulluk platform is a symmetrical structure, and the incoming directions of waves range from 0° to 180° at 15° intervals. The calculation period of waves ranges from 2 s to 38 s, and relevant data of 6 degrees of freedom motions are observed. In the subsequent time-domain calculation, the load direction of 180° is mainly analyzed. In this case, the surge and pitch motions are most representative. Therefore, only these two motions are selected in the analysis. Parts of the calculation results are seen in Figure 10.

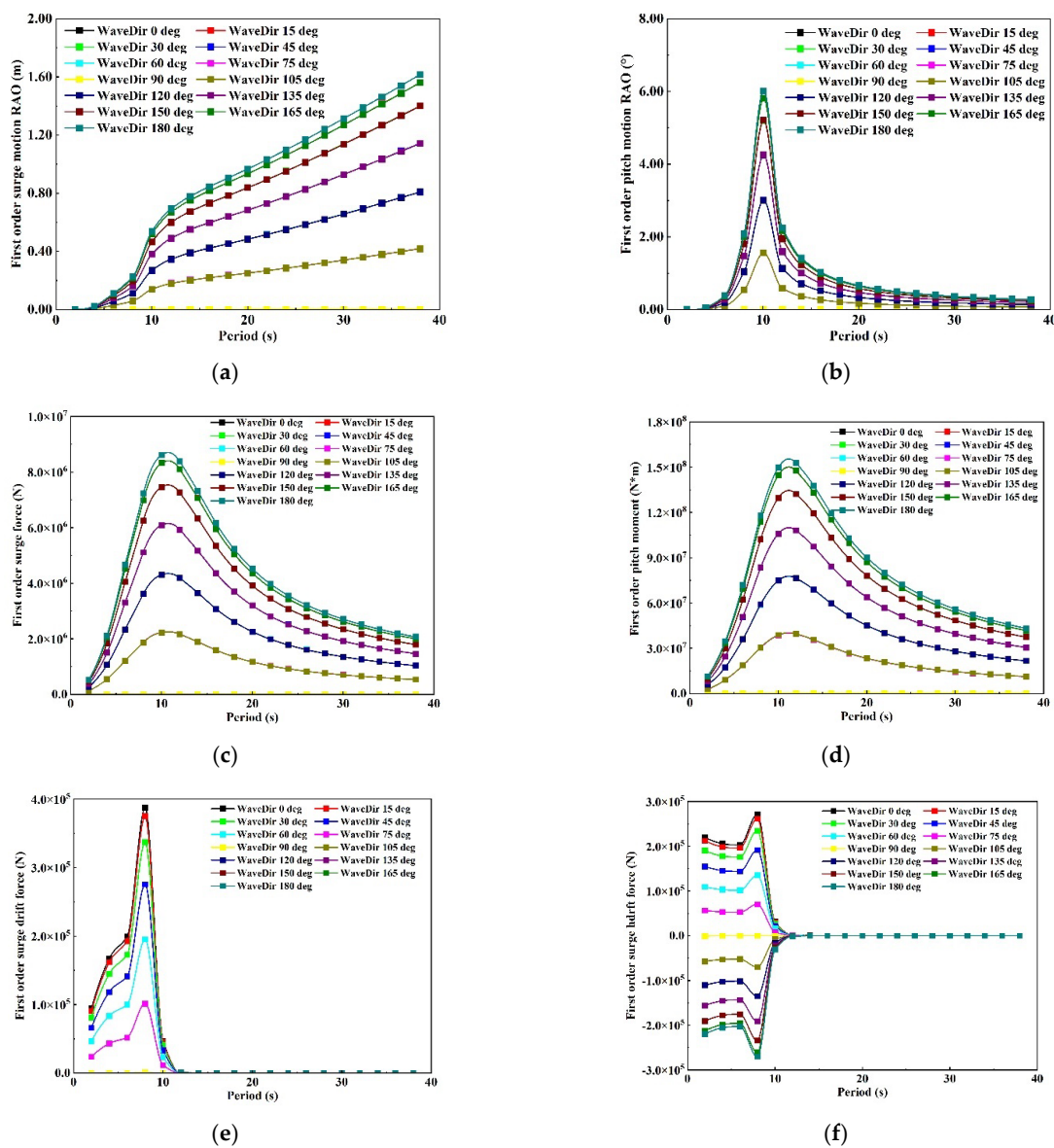


Figure 10. Calculation results of hydrodynamic analysis of the Kulluk platform. (a) First-order surge motion transfer function RAO; (b) first-order pitch motion transfer function RAO; (c) first-order surge force; (d) first-order pitch moment; (e) mean drift force in the surge by far-field method; (f) mean drift force in the surge by direct pressure integral method.

6. Ice Load Calculation of the Kulluk Platform

The ice load of the Kulluk platform is analyzed by the discrete element method. Figure 11 demonstrates the simulation process of the platform under conditions of level ice and broken ice floes. The calculation conditions are shown in Section 4. Figure 11c,d shows the failure mode of ice in contact with structure. This paper compares the numerical calculation results with the field data [3] from two aspects of ice thickness and ice concentration. The original Kulluk load event data are usually for broken ice floes, as during actual offshore operations, ice management will avoid large-sized level ice coming into contact with the platform. It can be seen from Figure 12 that the numerical results under the calculation conditions of broken ice floes are close to the field data and satisfy the upper limit of ice load specified by the linear equation in the Kulluk research report. To sum up, the calculated data in this paper are reasonable within the range of the field data and can be applied for subsequent calculations.

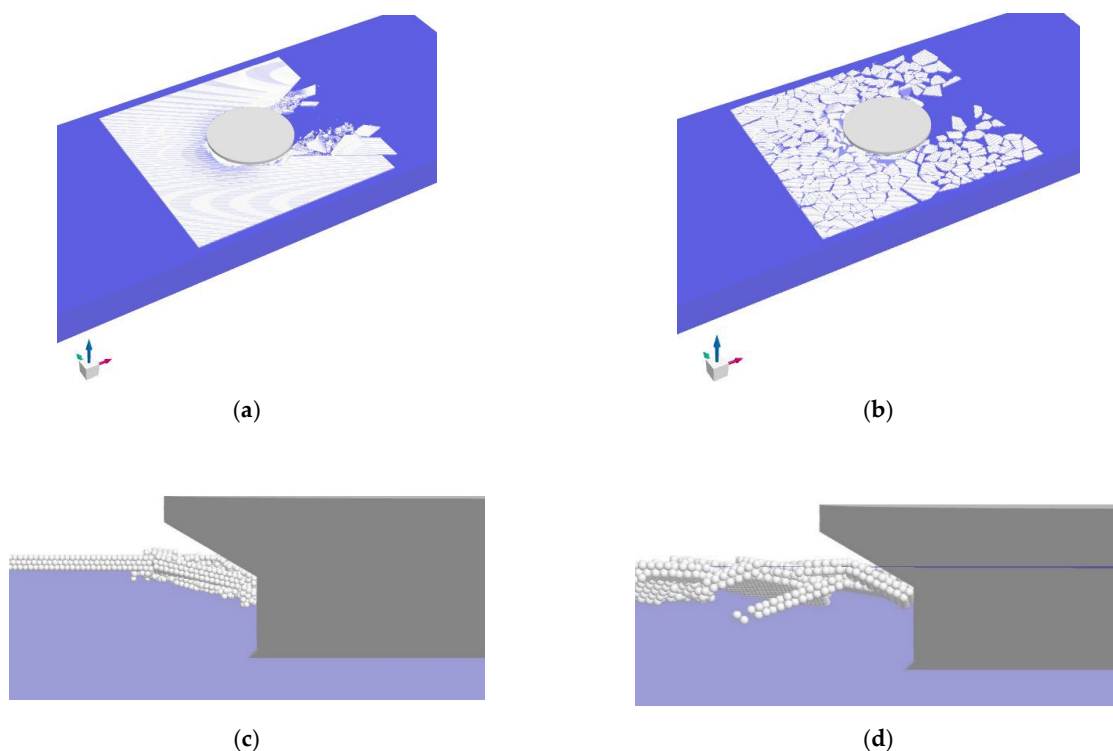


Figure 11. Numerical simulation of ice load on Kulluk platform. (a) Level ice condition; (b) broken ice floes condition; (c) front view under level ice condition; (d) front view under broken ice floes condition.

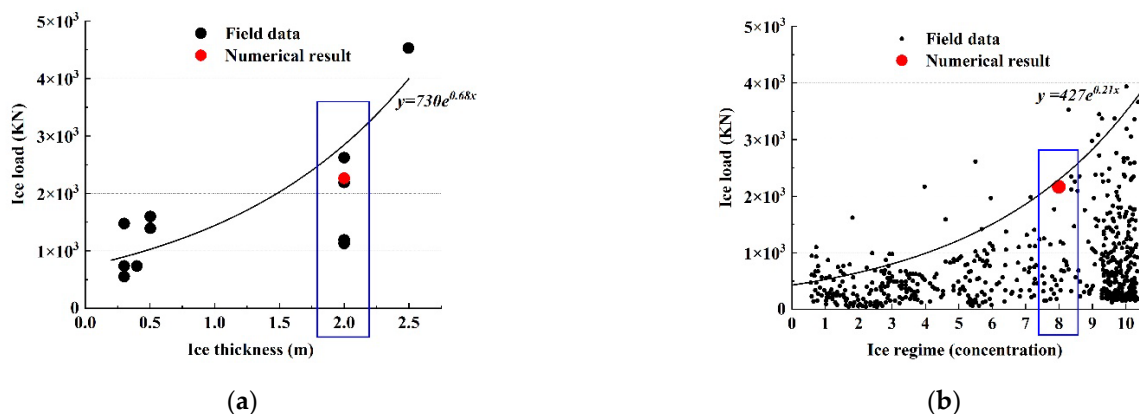


Figure 12. Comparison between the numerical simulation results and the field data of the Kulluk platform. (a) Ice thickness as the independent variable; (b) ice concentration as the independent variable.

7. Results and Discussion

This paper takes the mooring system design as the research object. The incidence angle of environmental loads, the number of mooring lines, the number of connection points, and the angle between mooring lines are all factors to be concerned about to complete the design of an optimal mooring system. The dynamic response under different working conditions of the wave, level ice, and broken ice floes is analyzed from two aspects, including mooring line tension and platform motion. In the time-domain simulation analysis, the computation time is 1800 s.

7.1. Influence of Load Direction on Mooring System

This paper analyzes the effect of load incidence angle on the coupling system by regarding the layout of four mooring lines as an example. Considering the symmetry of the Kulluk platform, four different load directions of 180°, 165°, 150°, and 135° are selected for study, as shown in Figure 13. By comparing the mean value and maximum value of mooring line tension under wave load, level ice load, and broken ice floes load, it can be seen that the tension of the mooring line with the largest force changes little under different load incidence angles. Figure 14 indicates the tension comparison of all mooring lines under different load directions. Compared with wave loads and broken ice floes in different directions, level ice in different directions have more obvious effects on mooring line tension. Mooring line 1 has the highest tension. Under wave loads, the maximum tension and average tension of mooring line 1 change by 4.58% and 0.62%, respectively. Under level ice, the maximum and average tension of mooring line 1 changed by 26.56% and 3.45%, respectively. The maximum and average tension of mooring line 1 changed by 11.11% and 4.63%, respectively, under broken ice floes. Therefore, the influence of load direction is not considered in the follow-up study.

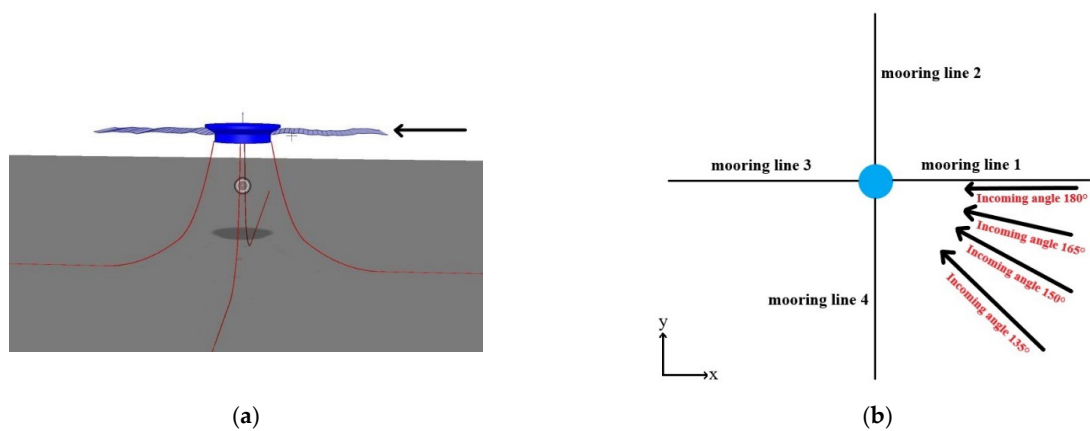


Figure 13. Influence of load direction on mooring system. (a) The coupled system for analysis; (b) schematic diagram of different load directions.

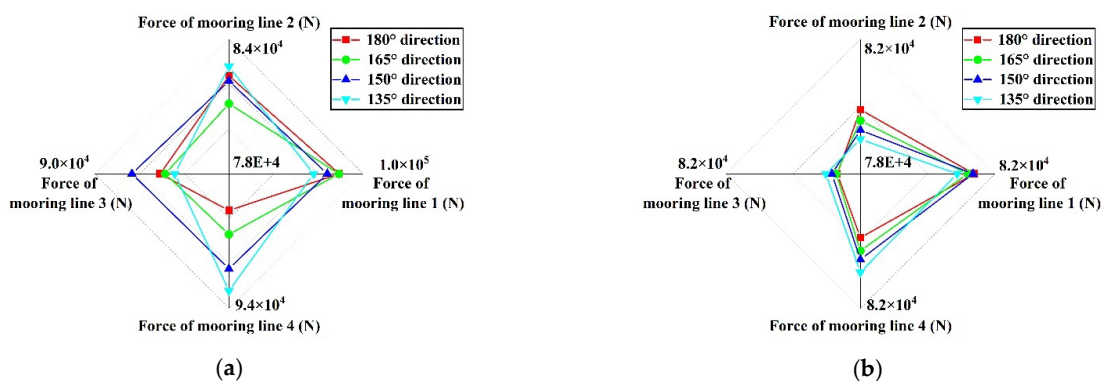


Figure 14. Cont.

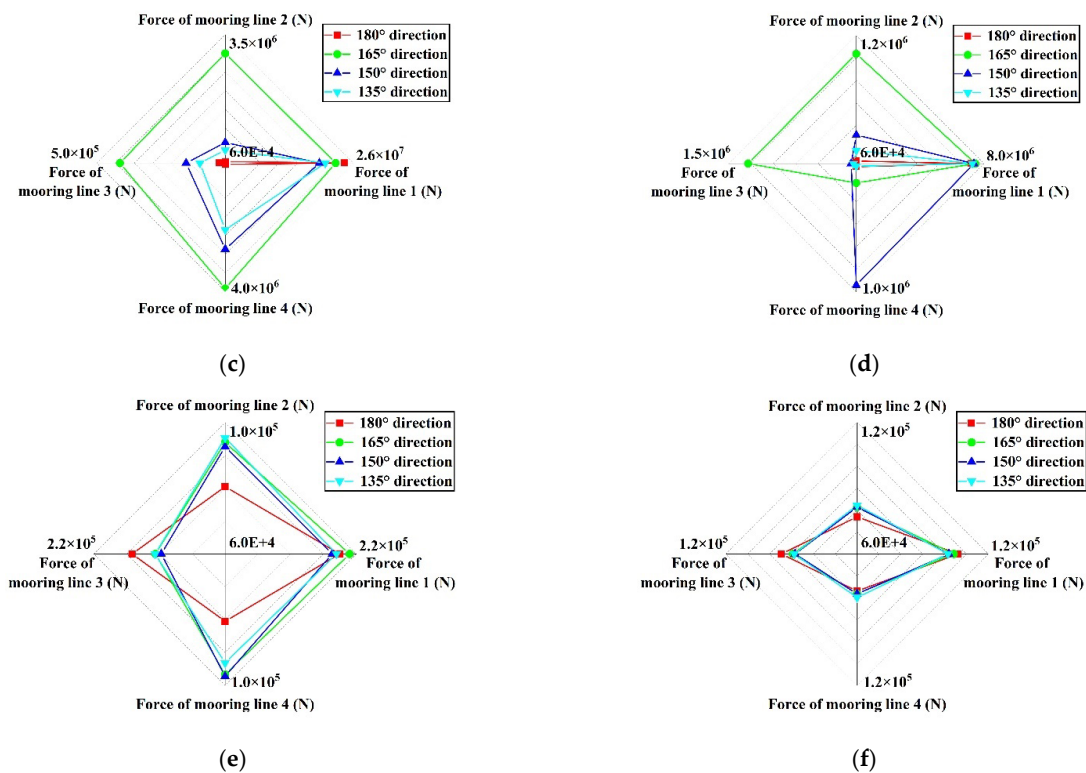


Figure 14. Tension comparison of four mooring lines under different load directions. (a) Maximum tension of mooring lines under wave loads; (b) mean tension of mooring lines under wave loads; (c) maximum tension of mooring lines under level ice loads; (d) mean tension of mooring lines under level ice loads; (e) maximum tension of mooring lines under broken ice floes loads; (f) mean tension of mooring lines under wave loads.

7.2. Influence of the Number of Mooring Lines on the Mooring System

In this paper, different configurations of four mooring lines, eight mooring lines, and twelve mooring lines are selected to investigate the influence of the number of mooring lines. These three designs are all arranged symmetrically, and the length and stiffness of the mooring lines are the same. The incidence angle of the environmental load is 180° . Figure 15 depicts the specific layout of the mooring system. Besides surge motion and pitch motion of the platform, the maximum tension and the mean tension of the mooring system are compared. The tension of the mooring system is defined as the force evenly distributed to each mooring line, which can reflect the overall level of mooring line tension in this design. The tension of mooring line 1 under time-domain analysis must also be compared. Mooring line 1 is subjected to the most tremendous tension in the mooring system. The segment connected with fairlead is selected for analysis. The results are shown in Figure 16. Under wave load and broken ice floes, the slightest tension on the mooring system is the design of eight mooring lines. Under the level ice load, the optimal design is twelve mooring lines. The tension of mooring lines in the configuration of four mooring lines is much greater than that in the other two designs under ice loads. Under the condition of level ice, the maximum tension and mean tension of four mooring lines design increases by 126.68% and 98.64% compared with the eight-mooring-line design as well as 252.89% and 167.21% compared with the twelve-mooring-line design. Under broken ice floes, these values are 63.29%, 53.49%, 27.98%, and 10.18%, respectively. This reveals that the mooring line of the four-mooring-line design makes it easier to attain the design stiffness. Its safety is not as good as the other two designs in the case of mooring line fracture. It is also verified by the time-domain analysis of mooring line 1. Meanwhile, it can be seen that under the design mode of twelve mooring lines, the tension of mooring line 1 is the least. The results are all similar in the conditions of the wave, level ice, and broken ice floes.

The motions of the platform are described in Figure 17. There are apparent differences in surge motion under the three design modes. Under wave load, the maximum platform surge motion with twelve mooring lines is 224.43% and 138.51% smaller than that with four mooring lines and eight mooring lines, respectively. Under level ice, surge motion of the twelve-mooring-line design decreases by 10.92% and 7.27%, respectively. Surge motion decreases by 286.09% and 86.14% under broken ice floes. There is little distinction in pitch motion, and the mooring system’s positioning effect, which is composed of twelve mooring lines, is the best.

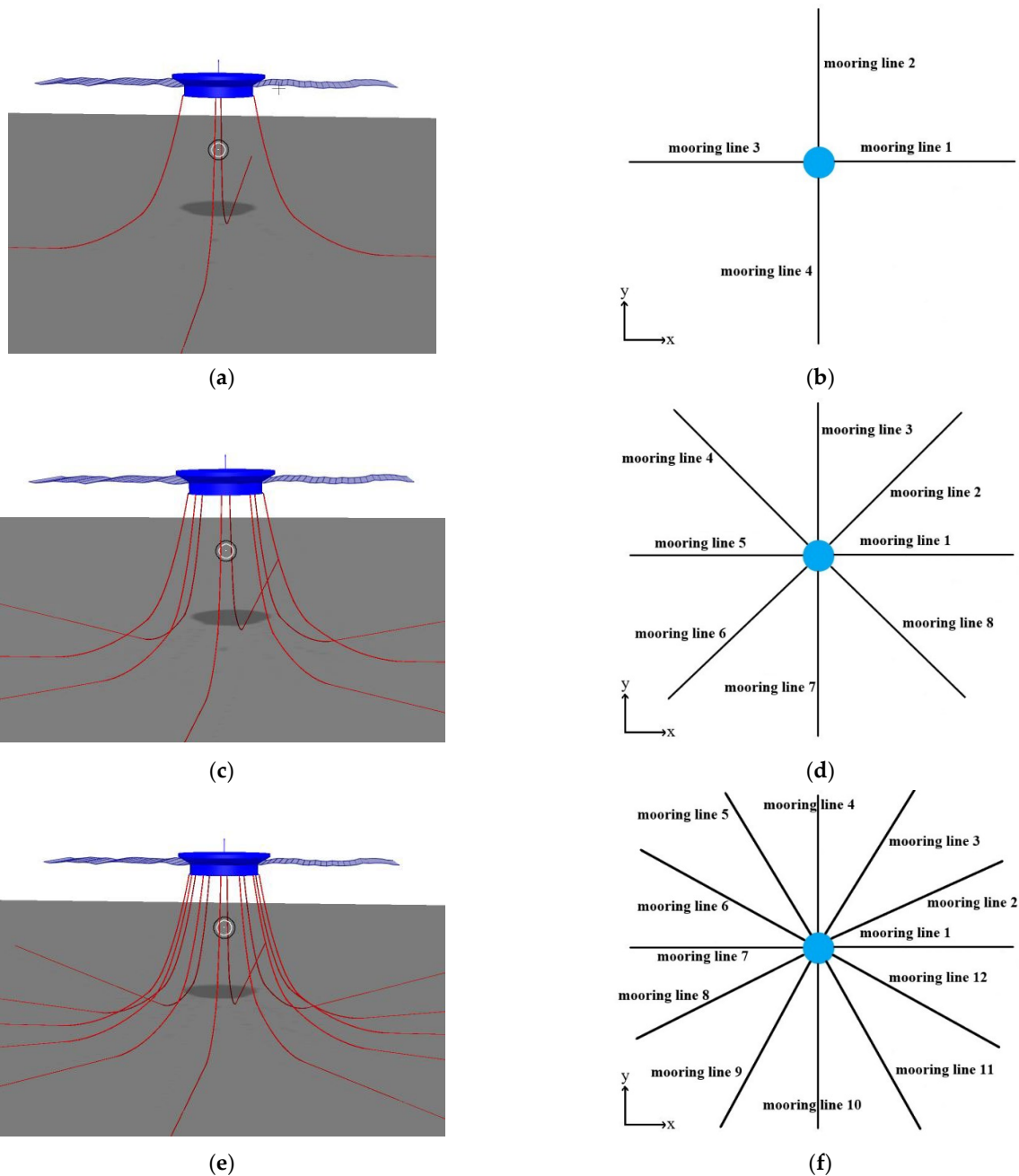


Figure 15. Influence of the number of mooring lines on the mooring system. (a) The coupled system for analysis with four mooring lines; (b) schematic diagram of the design of four mooring lines; (c) the coupled system for analysis with eight mooring lines; (d) schematic diagram of the design of eight mooring lines; (e) the coupled system for analysis with twelve mooring lines; (f) schematic diagram of the design of twelve mooring lines.

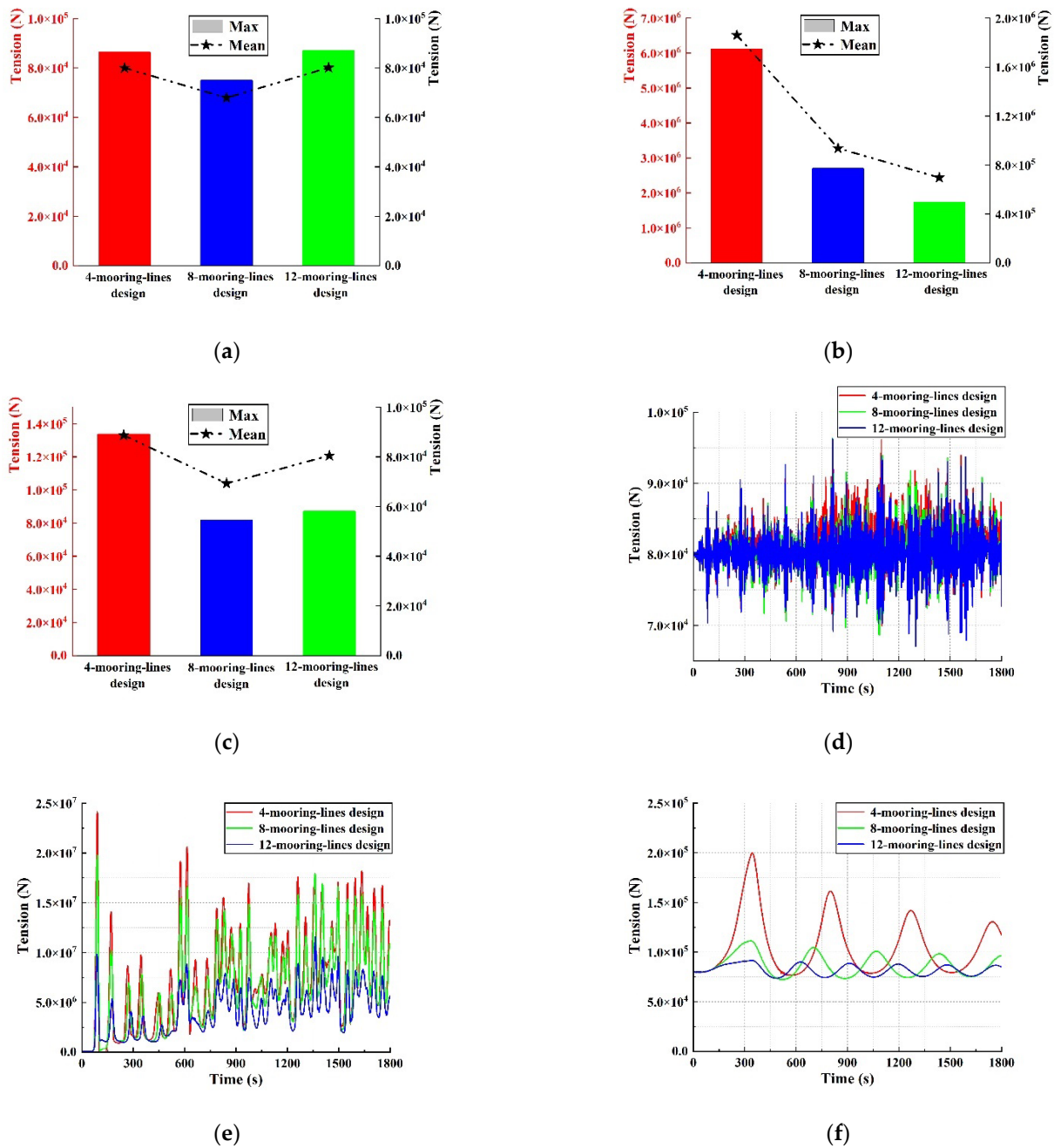


Figure 16. Influence of the number of mooring lines on mooring line tension. (a) Maximum and mean values of mooring system tension under wave loads; (b) maximum and mean values of mooring system tension under level ice loads; (c) maximum and mean values of mooring system tension under broken ice floes loads; (d) the tension of mooring line 1 under wave loads in time-domain analysis; (e) the tension of mooring line 1 under level ice loads in time-domain analysis; (f) the tension of mooring line 1 under broken ice floes loads in time-domain analysis.

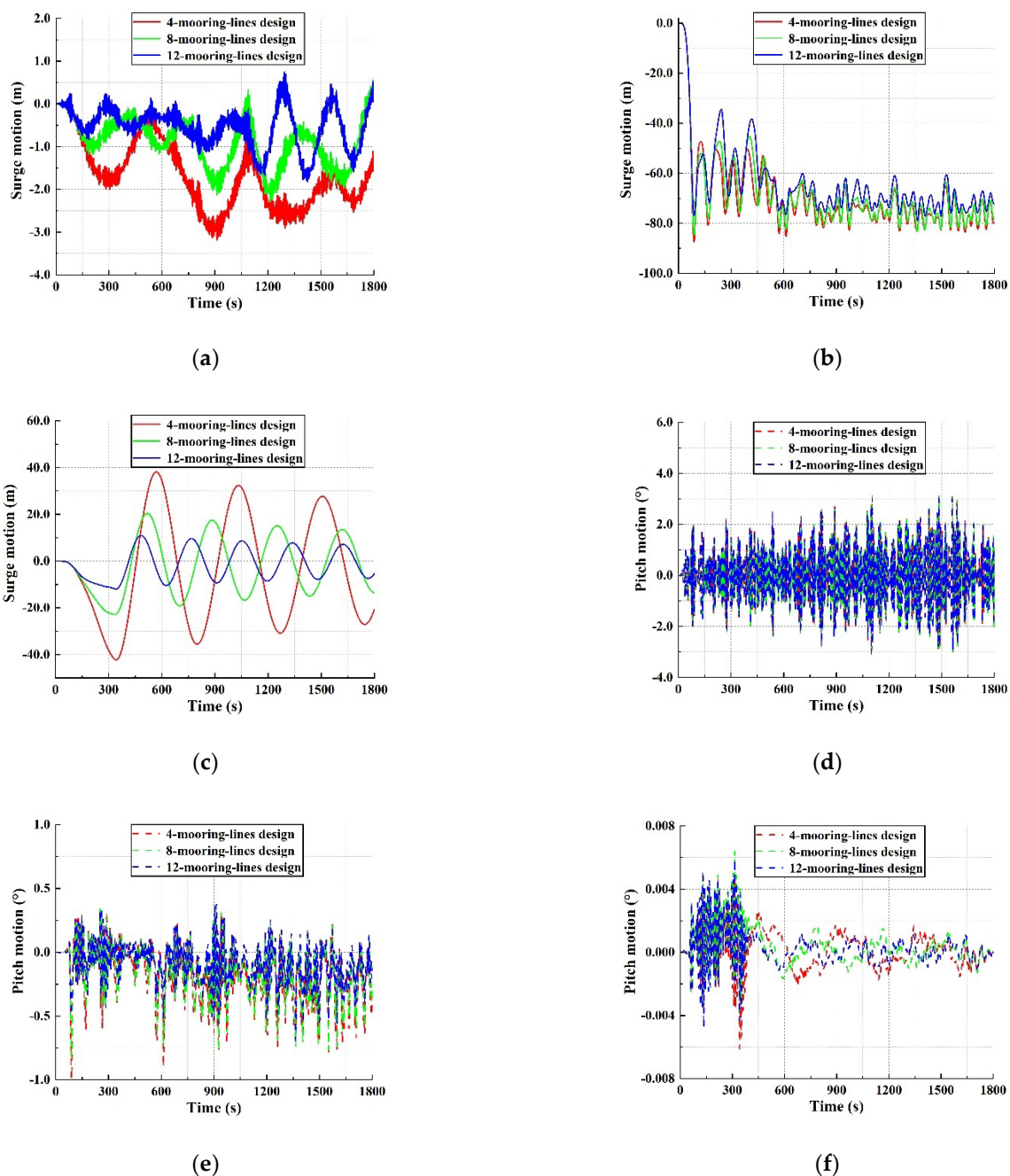


Figure 17. Influence of the number of mooring lines on Kulluk platform motion. (a) Surge motion under wave loads; (b) surge motion under level ice loads; (c) surge motion under broken ice floes loads; (d) pitch motion under wave loads; (e) pitch motion under level ice loads; (f) pitch motion under broken ice floes loads.

7.3. Influence of the Number of Connection Points on the Mooring System

In this paper, three different designs are selected to analyze the influence of the number of connection points on the mooring system, including one connection point, four connection points, and twelve connection points. Twelve symmetrical mooring lines are adopted for the study, and the loading direction is 180° . The one-connection-point design means that all mooring lines are connected to the Kulluk through the same fairlead. The layout of the four connection points is unique, and each of the three mooring lines shares the same fairlead. The angle between the mooring lines on both sides and the middle one is 30° . Figure 18 describes the specific arrangement of various connection

point designs. The analysis results of mooring line tension and platform motion are demonstrated in Figures 19 and 20. Each mooring line tension of the one-connection-point design is more significant than that of the other two design methods under the wave, level ice, and broken ice floes. By comparing the tension of mooring line 1, surge motion, and pitch motion of the platform in time-domain analysis, it can be seen that the dynamic response of the coupled system does not have a significant difference under the design of four connection points and twelve connection points. Considering practical construction requirements such as operability, schedule, and cost, the four-connection-point design is a more suitable arrangement.

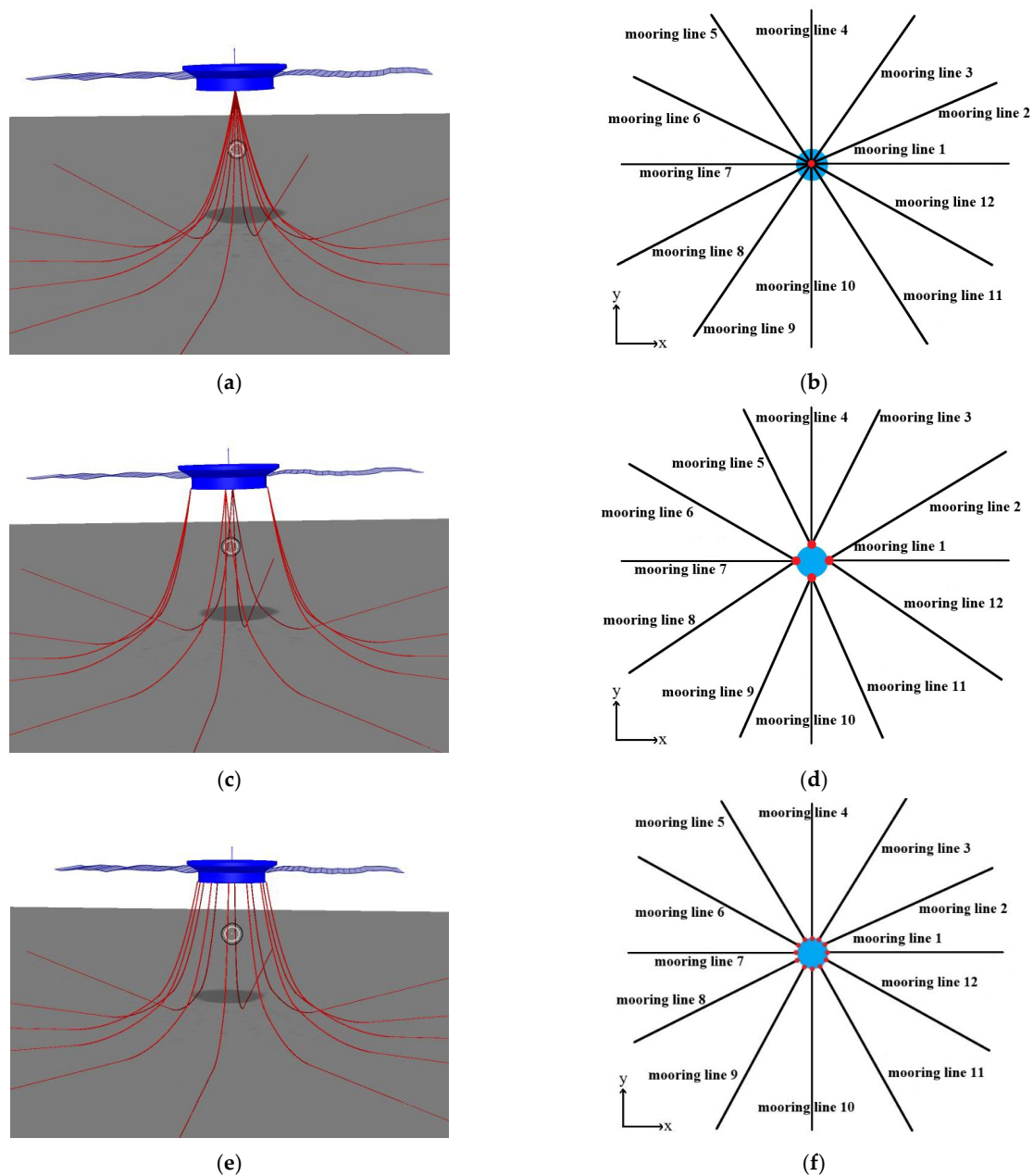


Figure 18. Influence of the number of connection points on the mooring system. (a) The coupled system for analysis with one connection point; (b) schematic diagram of the design of one connection point; (c) the coupled system for analysis with four connection points; (d) schematic diagram of the design of four connection points; (e) the coupled system for analysis with twelve connection points; (f) schematic diagram of the design of twelve connection points.

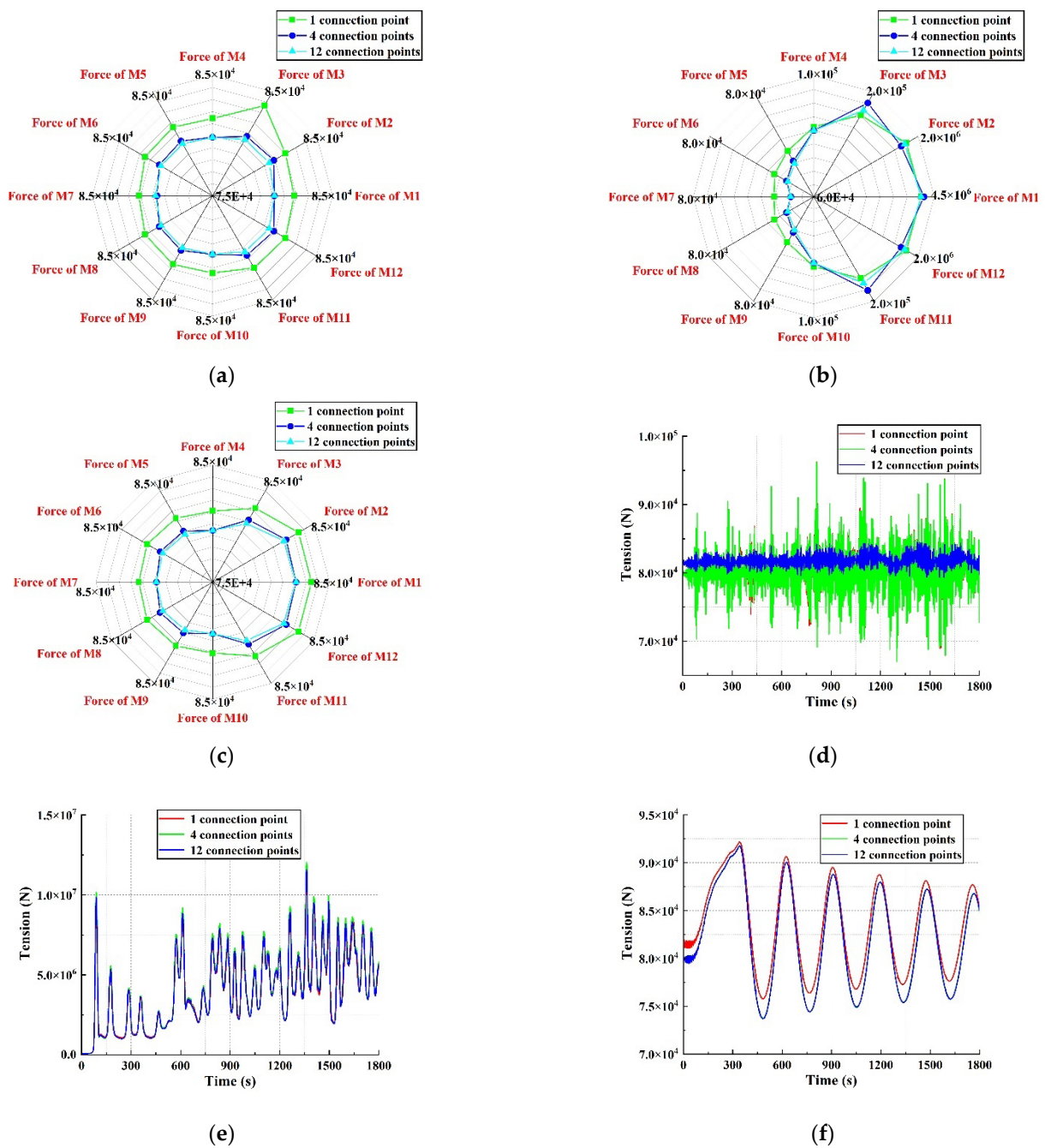


Figure 19. Influence of the number of connection points on mooring line tension. (a) Mean tension of mooring lines under wave loads; (b) mean tension of mooring lines under level ice loads; (c) mean tension of mooring lines under broken ice floes loads; (d) the tension of mooring line 1 under wave load in time-domain analysis; (e) the tension of mooring line 1 under level ice load in time-domain analysis; (f) the tension of mooring line 1 under broken ice floes load in time-domain analysis.

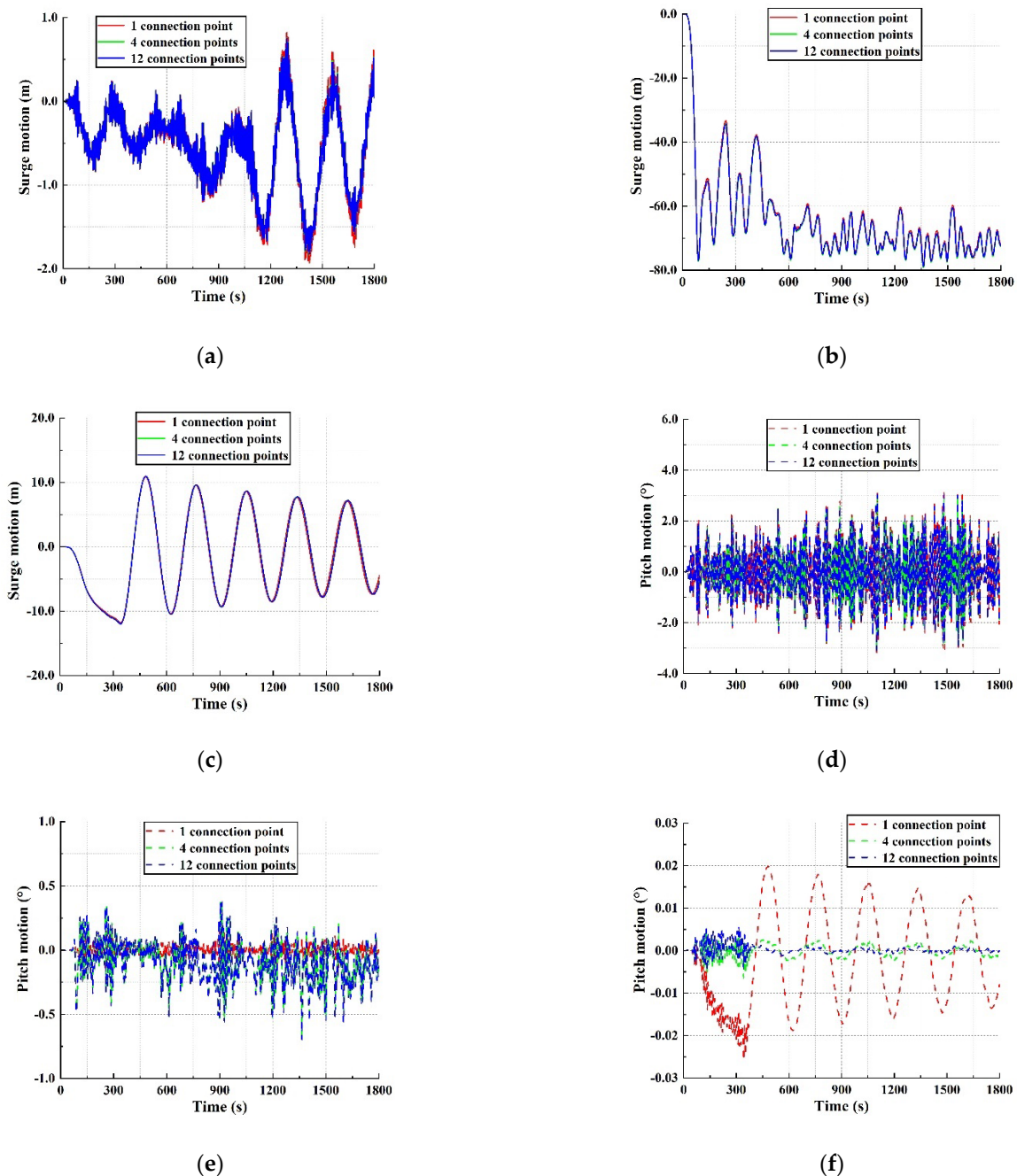


Figure 20. Influence of the number of connection points on Kulluk platform motion. (a) Surge motion under wave loads; (b) surge motion under level ice loads; (c) surge motion under broken ice floes loads; (d) pitch motion under wave loads; (e) pitch motion under level ice loads; (f) pitch motion under broken ice floes loads.

7.4. Influence of the Angle between Mooring Lines on the Mooring System

In this paper, three different angles of 10° , 20° , and 30° are selected for numerical simulation. The mooring system has twelve mooring lines and four connecting points. The loading direction is 180° . The specific arrangement of mooring lines is presented in Figure 21. The mooring system's mean tension is very close in these three designs. The mooring system's maximum tension varies slightly as well. Under the condition of level ice, the 10° design minimizes the tension of mooring line 1. In most cases, these three different angles have quite little influence on the platform motions, which are similar numerically. The motion response curves of the time-domain analysis are almost identical. Only in the

platform surge motion under level ice conditions and the platform pitch motion under broken ice floes conditions can it be seen that 10° is the best angle between the mooring lines. The calculation results are shown in Figures 22 and 23.

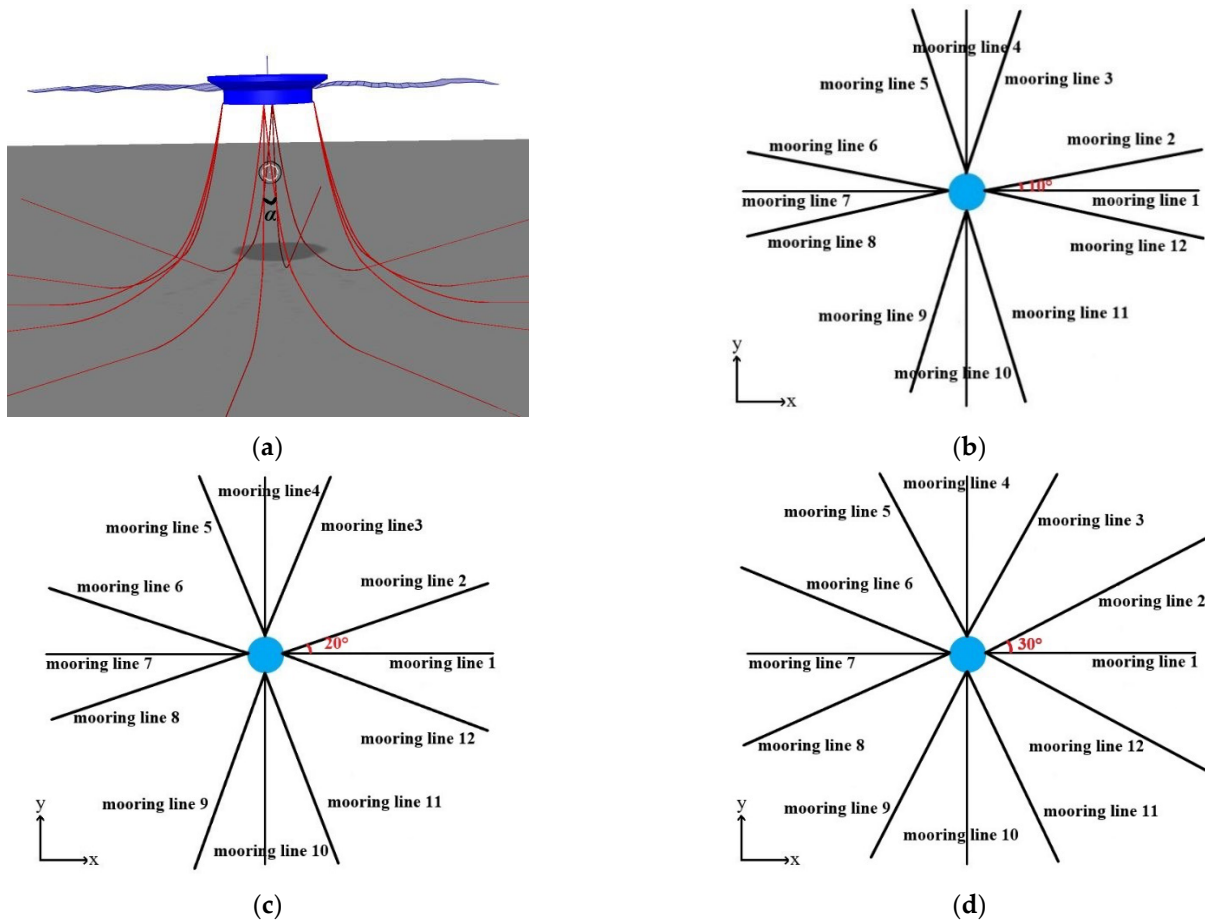


Figure 21. Influence of the angle between mooring lines on the mooring system. (a) The coupled system for analysis; (b) schematic diagram of the design of 10° between mooring lines; (c) schematic diagram of the design of 20° between mooring lines; (d) schematic diagram of the design of 30° between mooring lines.

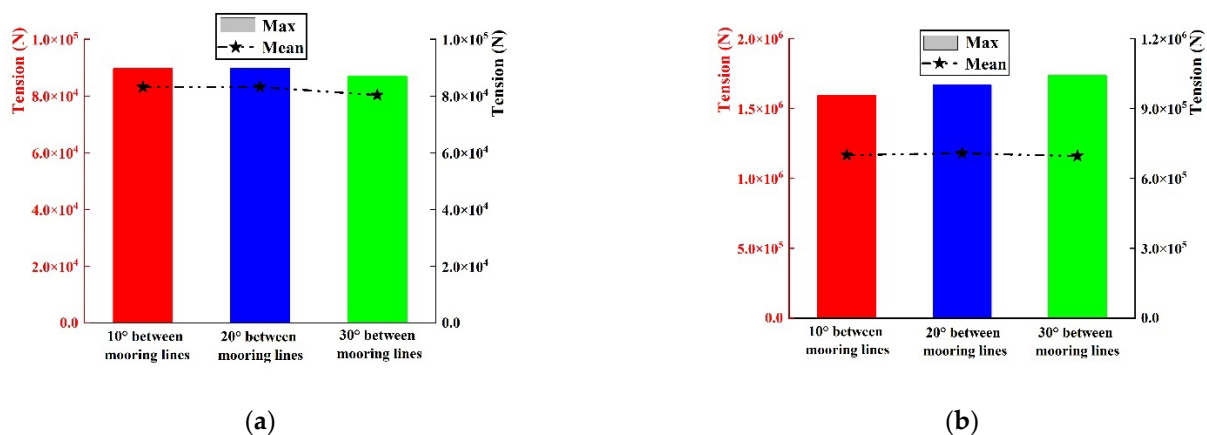
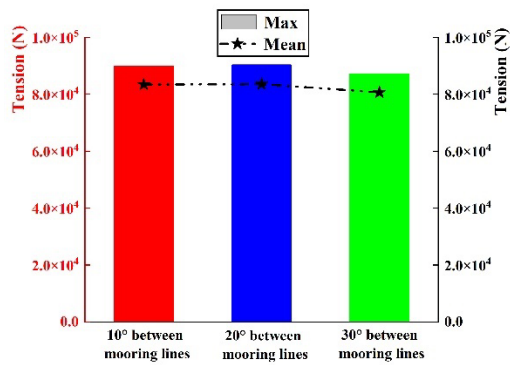
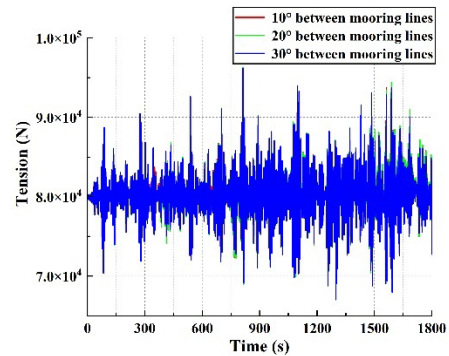


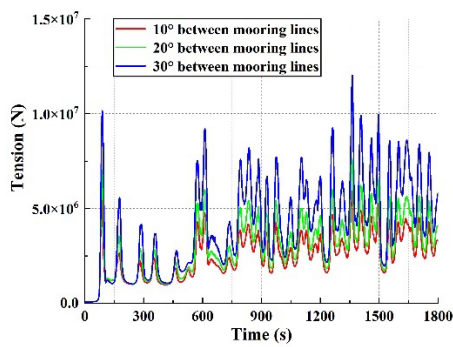
Figure 22. Cont.



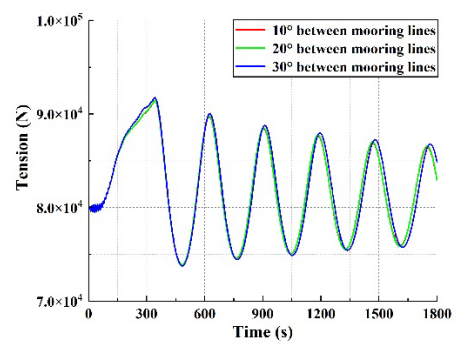
(c)



(d)

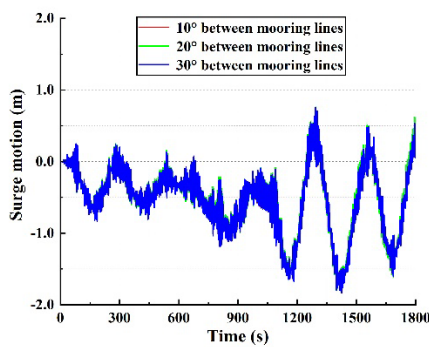


(e)

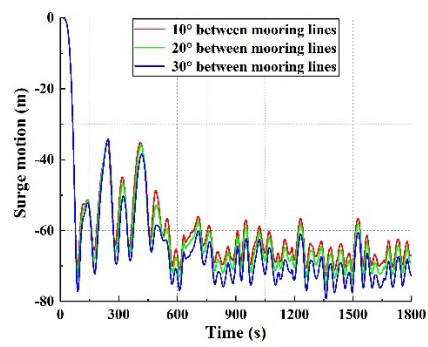


(f)

Figure 22. Influence of the angle between mooring lines on mooring line tension. (a) Maximum and mean values of mooring system tension under wave loads; (b) maximum and mean values of mooring system tension under level ice loads; (c) maximum and mean values of mooring system tension under broken ice floes loads; (d) the tension of mooring line 1 under wave load in time-domain analysis; (e) the tension of mooring line 1 under level ice load in time-domain analysis; (f) the tension of mooring line 1 under broken ice floes load in time-domain analysis.



(a)



(b)

Figure 23. Cont.

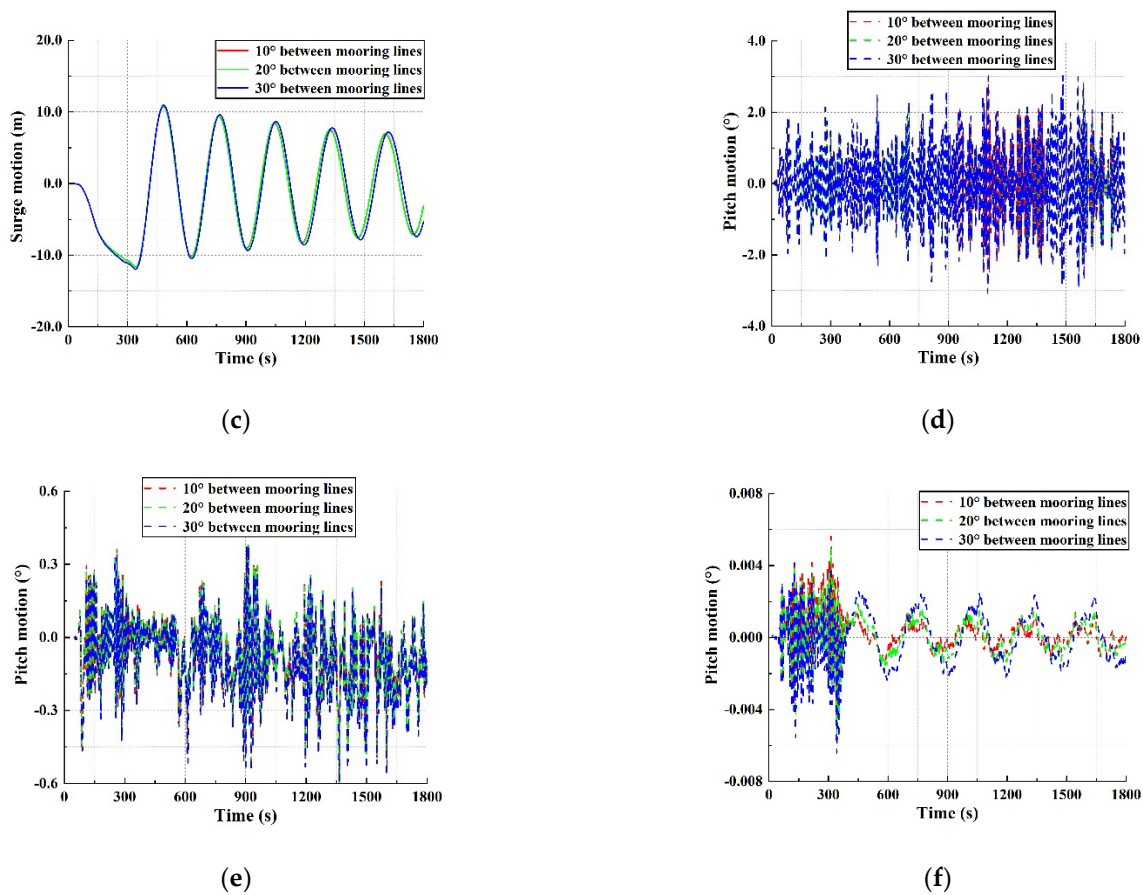


Figure 23. Influence of the angle between mooring lines on Kulluk platform motion. (a) Surge motion under wave loads; (b) surge motion under level ice loads; (c) surge motion under broken ice floes loads; (d) pitch motion under wave loads; (e) pitch motion under level ice loads; (f) pitch motion under broken ice floes loads.

In order to verify whether there is a better design scheme when the angle is less than 10° , the surge motion of the platform under level ice and the pitch motion under broken ice floes are compared when the angles between mooring lines are 5° , 7.5° , and 10° . The results are so close that there is no significant difference, as displayed in Figure 24. In order to avoid collision or entanglement between mooring lines caused by too close a distance, the angle between mooring lines is finally determined to be 10° .

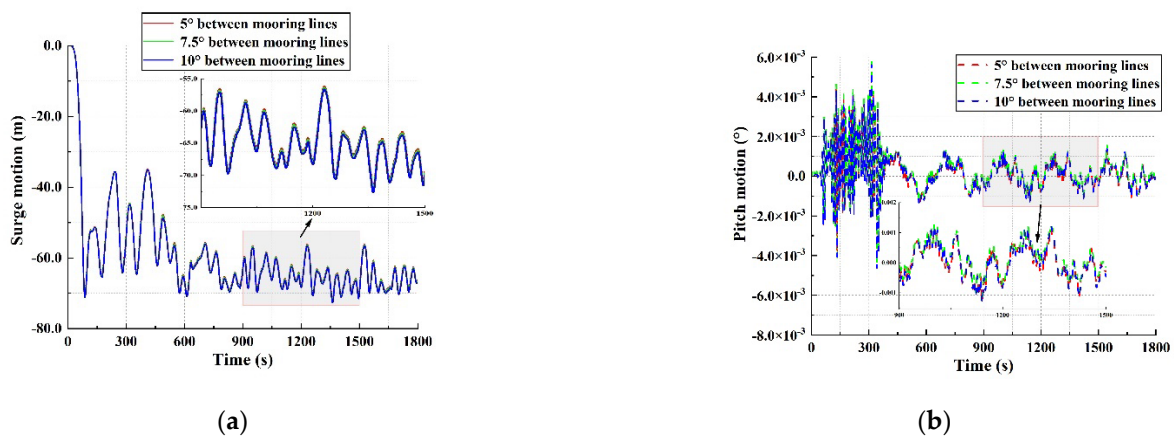


Figure 24. Comparison of three groups of mooring lines with angles of 5° , 7.5° , and 10° . (a) Surge motion under level ice loads; (b) pitch motion under broken ice floes loads.

8. Conclusions

In order to find the relevant factors affecting the mooring system and optimize the mooring line layout of the Kulluk platform, this paper simulates the dynamic response of the Kulluk platform during ice-free and ice-covered seasons in the Beaufort Sea. Statistical and nonlinear time-domain simulation methods analyze the tension of mooring lines and the platform's motion. Different working conditions such as wave load, level ice load, and broken ice floes load are taken into account. The findings are drawn as follows:

The empirical formula, nonlinear finite element method, and discrete element method are standard methods for computing ice loads. In this paper, by calculating the cylindrical structure and the cone structure, it can be seen that the nonlinear finite element method is closer to the empirical formula in the analysis of crushing failure. The discrete element method is more suitable for calculating the flexure failure of ice. The ice load of the Kulluk platform is analyzed by the discrete element method because the contact position between the Kulluk platform and the ice is a slope. The calculated results are consistent with the field data, which proves the accuracy of the numerical simulation.

- (1) The influence of level ice load on platform motion and mooring system tension is much more significant than that of wave and broken ice floes load. Ongoing ice management exists in actual offshore operations. It can control loads of the mooring lines and keep the mooring system's tension and the platform's motion within an acceptable range.
- (2) For the dynamic response of the mooring system of the Kulluk platform, the load direction is not the decisive factor. The number of mooring lines, the number of connecting points, and the angle between the mooring lines all affect the tension of the mooring lines and the platform's motion to a certain extent. Mooring lines with more numbers have the best positioning effect, and each mooring line has the lowest tension and the highest safety. When the dynamic response difference is less than 1%, the final design is determined based on the actual construction costs and offshore operations conditions.
- (3) The final design scheme is determined as twelve mooring lines, four connecting points, and with an angle between the mooring lines of 10° . Under wave and broken ice floes conditions, the surge motion of the coupling system is less than 10% of the working water depth, and the pitch motion is less than 5° , which well satisfies the relevant design requirement of offshore platforms. The platform is suitable for both ice-free and ice-covered seasons and can be used for year-round offshore operations.

In the following research, this method will be applied to the thruster-assisted mooring system and to optimize the positioning system of floating structures operating in cold regions except for offshore platforms.

Author Contributions: Conceptualization, Z.C. and S.L. (Shewen Liu); methodology, A.Z.; software, A.Z., Z.H. and S.L. (Shiqi Liu); validation, Z.C. and X.C.; formal analysis, S.L. (Shewen Liu); investigation, A.Z.; resources, Z.C.; data curation, A.Z.; writing—original draft preparation, A.Z.; writing—review and editing, Z.C.; visualization, L.H.; supervision, S.L. (Shewen Liu); project administration, Z.C.; funding acquisition, S.L. (Shewen Liu). All authors have read and agreed to the published version of the manuscript.

Funding: This research was funded by the Dalian Science and Technology Innovation Fund Project, grant number 2020JJ25CY016; the State Key Laboratory of Coastal and Offshore Engineering Fund, grant number LP2115 and Fundamental Research Funds for the Central University, grant number 3132022122.

Data Availability Statement: All analyzed data in this study have been included in the manuscript.

Acknowledgments: The authors would like to thank the Dalian Maritime University (DMU).

Conflicts of Interest: The authors declare no conflict of interest.

References

- Hamilton, J.M. The Challenges of Deep-Water Arctic Development. In Proceedings of the Twenty-First International Offshore and Polar Engineering Conference, Maui, HI, USA, 19–24 June 2011.
- Donald, L.G.; Kenneth, J.B.; Ronald, R.C.; Arthur, G.; David, W.H.; Timothy, R.K.; Thomas, E.M.; Janet, K.P.; Christopher, J.S.; John, H.S.; et al. Assessment of undiscovered oil and gas in the Arctic. *Science* **2009**, *324*, 1175–1179.
- Wright, B. Full Scale Experience with Kulluk Stationkeeping Operations in Pack Ice (With Reference to Grand Banks Developments). In *PERD/CHC Report 25–44*; National Research Council: Ottawa, ON, Canada, 2000.
- Zhou, L.; Su, B.; Riska, K.; Moan, T. Numerical simulation of moored structure station keeping in level ice. *Cold Reg. Sci. Technol.* **2012**, *71*, 54–66. [[CrossRef](#)]
- Sayed, M.; Barker, A. Numerical Simulations of Ice Interaction with a Moored Structure. In Proceedings of the Offshore Technology Conference, Houston, TX, USA, 2–5 May 2011.
- Wang, J.Y.; Derradji-Aouat, A. Numerical assessment for stationary structure (Kulluk) in moving broken ice. In Proceedings of the 21st International Conference on Port and Ocean Engineering under Arctic Conditions, POAC, Montréal, QC, Canada, 10–14 July 2011.
- Du, J.F.; Chang, A.T.; Wang, S.Q.; Sun, M.Y.; Wang, J.R.; Li, H.J. Multi-mode reliability analysis of mooring system of deep-water floating structures. *Ocean. Eng.* **2019**, *192*, 106517. [[CrossRef](#)]
- Garrett, D.L. Coupled analysis of floating production systems. *Ocean. Eng.* **2005**, *32*, 802–816. [[CrossRef](#)]
- Montasir, O.A.; Yenduri, A.; Kurian, V.J. Effect of mooring line configurations on the dynamic responses of truss spar platforms. *Ocean. Eng.* **2015**, *96*, 161–172. [[CrossRef](#)]
- Mohapatra, S.C.; Guedes Soares, C. Effect of Mooring Lines on the Hydroelastic Response of a Floating Flexible Plate Using the BIEM Approach. *J. Mar. Sci. Eng.* **2021**, *9*, 941. [[CrossRef](#)]
- Horrigmoe, G.; Andersen, R. Nonlinear finite element analysis of ice-structure interaction at varying strain rates. In Proceedings of the Fourth International Offshore and Polar Engineering Conference, Osaka, Japan, 10–15 April 1994.
- Edmond, H.H.; Sveinung, L. Modelling floating offshore units moored in broken ice: Comparing simulations with ice tank tests. *Cold Reg. Sci. Technol.* **1999**, *29*, 107–119.
- Liu, Z.H.; Jørgen, A.; Sveinung, L. Plasticity based material modelling of ice and its application to ship–iceberg impacts. *Cold Reg. Sci. Technol.* **2011**, *65*, 326–334. [[CrossRef](#)]
- Liu, L.; Ji, S.Y. Ice load on floating structure simulated with dilated polyhedral discrete element method in broken ice field. *Appl. Ocean. Res.* **2018**, *75*, 53–65. [[CrossRef](#)]
- Peyrot, A.H.; Goulois, A.M. Analysis of Cable Structures. *Comput. Struct.* **1979**, *10*, 805–813.
- Sødahl, N. *Design and Analysis of Flexible Risers*; The Norwegian Institute of Technology: Trondheim, Norway, 1991.
- Faltinsen, O.M. *Sea Loads on Ships and Offshore Structures*; Cambridge University Press: Cambridge, UK, 1990.
- DNV. Sesam User Manual Sesam Manager. 2018. Available online: https://www.dnv.com/services/strength-assessment-of-offshore-structures-sesam-software-1068?utm_campaign=structure_sesam&utm_source=google&utm_medium=cpc&gclid=EAIaIQobChMIInITk2sGE-AIVAcuWCh3XcQyxEAAYASAAEgKNB_D_BwE&gclsrc=aw.ds (accessed on 15 May 2022).
- DNV. SESAM User Manual WADAM. DNV Software Report No.: 92-7052. 2017. Available online: https://www.dnv.com/services/strength-assessment-of-offshore-structures-sesam-software-1068?utm_campaign=structure_sesam&utm_source=google&utm_medium=cpc&gclid=EAIaIQobChMIInITk2sGE-AIVAcuWCh3XcQyxEAAYASAAEgKNB_D_BwE&gclsrc=aw.ds (accessed on 15 May 2022).
- SINTEF Ocean. SIMO 4.16.0 User Guide. 11 May 2019. Available online: https://sesam.dnv.com/status/simo/status/simo-release-notes_4.16.1.pdf (accessed on 15 May 2022).
- Zhang, A.B.; Chuang, Z.J.; Liu, S.W.; Zhou, L.; Qu, Y.; Lu, Y. Dynamic performance optimization of an arctic semi-submersible production system. *Ocean. Eng.* **2022**, *244*, 110353. [[CrossRef](#)]
- ISO 19906; Petroleum and Natural Gas Industries-Arctic Offshore Structures. 2nd ed. ISO: Geneva, Switzerland, 2019.
- Hallquist, J.O. *LS-DYNA Theoretical Manual*; Livermore Software Technology Corporation: Livermore, CA, USA, 2006.
- Wang, C.; Hu, X.H.; Tian, T.P.; Guo, C.Y.; Wang, C.H. Numerical simulation of ice loads on a ship in broken ice fields using an elastic ice model. *Int. J. Nav. Archit. Ocean. Eng.* **2020**, *12*, 414–427. [[CrossRef](#)]
- Guo, C.Y.; Zhang, Z.T.; Tian, T.P.; Li, X.Y.; Zhao, D.G. Numerical simulation on the resistance performance of ice-going container ship under brash ice conditions. *China Ocean. Eng.* **2018**, *32*, 546–556. [[CrossRef](#)]
- Shen, H.H.; Hibler, W.D.; Lepparanta, M. On applying granular flow theory to a deforming broken ice field. *Acta Mech.* **1986**, *63*, 143–160. [[CrossRef](#)]
- Potyondy, D.O.; Cundall, P.A. A bonded-particle model for rock. *Int. J. Rock Mech. Min. Sci.* **2004**, *41*, 1329–1364. [[CrossRef](#)]
- Campbell, C.S. Stress-controlled elastic granular shear flows. *J. Fluid. Mech.* **2005**, *539*, 273–297. [[CrossRef](#)]
- Wang, Y.; Tonon, F. Calibration of a discrete element model for intact rock up to its peak strength. *Int. J. Numer. Anal. Methods Geomech.* **2010**, *34*, 447–469. [[CrossRef](#)]
- Mollon, G.; Zhao, J. Fourier–Voronoi-based generation of realistic samples for discrete modelling of granular materials. *Granul. Matter* **2012**, *14*, 621–638. [[CrossRef](#)]

31. Maruo, H. The drift of a body floating on waves. *J. Ship Res.* **1960**, *4*, 1–10.
32. Pinkster, J.A.; van Oortmerssen, G. Computation of the first and second-order wave forces on oscillating bodies in regular waves. In Proceedings of the 2nd International Conference on Numerical Ship Hydrodynamics, Berkeley, CA, USA, 19–21 September 1977; pp. 136–159.